Available online at www.sciencedirect.com
SCIENCE DIRECT
Lithos 89 (2006) 66–88
LITHOS
www.elsevier.com/locate/lithos

Genesis of aluminous and intermediate granulites: A case study in the eastern Sierras Pampeanas, Argentina

J.E. Otamendi [a,*], A.H. Demichelis [a], A.M. Tibaldi [a], J.D. de la Rosa [b]

[a] *Departamento de Geología, Universidad Nacional de Río Cuarto, X5804BYA Río Cuarto, Argentina*
[b] *Departamento de Geología, Universidad de Huelva, E21071 Huelva, Spain*

Received 1 October 2004; accepted 6 September 2005
Available online 17 November 2005

Abstract

We report petrologic and geochemical features of anhydrous granulites from the eastern Sierras Pampeanas, Argentina. Aluminous Grt–Crd-bearing granulite is the most abundant rock type in the study region, and hosts intermediate Opx–Grt bearing granulites as interlayered lenses. Both granulite types crystallized under similar *P–T* conditions of $T=850$–900 °C and P c. 7.5 kbar. The formation of Grt–Crd granulites by subsolidus dehydration conflicts with the absence of K-feldspar in them. Moreover, the aluminous granulites have an REE pattern that precludes postulating they derived by close-system metamorphism of an extensively weathered protoliths. Comparing mineral and rock chemistry with experimental results in simple systems (ACFM, AKF, and AFM) permits the mineralogical changes and the bulk composition evolution experienced by granulites during melting to be identified. This work demonstrates that orthopyroxene is a primary phase in Opx–Grt granulites, however never crystallized within aluminous granulites. The aluminous granulites have both mineral and chemical compositions matching those expected for a residuum derived from the partial melting of a greywacke-like sedimentary precursor. Compared with the composition of the average continental crust, aluminous granulites are depleted in most lithophile trace elements and LREE, have somewhat low K/Rb ratios, and high contents of elements having high partition coefficients for garnet and/or ilmenite (HREE—Y, Cr, Ni). However, aluminous granulites have initial Sr isotope ratios (<0.708) significantly lower than those measured in the rest of the metasedimentary rocks of the region (>0.713). We discuss the possibility that an intense but short-lived melting event led to isotopic disequilibrium during melting of biotite-bearing protoliths, leaving a granulitic residuum with lower initial Sr isotope ratios. In contrast, Opx–Grt granulites have trace element features (e.g., high Sr contents and REE patterns with marked positive Eu anomalies) that do not support the idea that they are simply residues left after biotite-dehydration melting and melt extraction. Rather, these rocks display several petrological, major and trace element and isotopic features that suggest they formed through the interaction of mafic magmas and aluminous granulites.

Keywords: Granulite; Partial melting; Crustal differentiation; Petrogenesis; Sierras Pampeanas

1. Introduction

Refractory granulites are an extreme petrologic product within the lineage of the supracrustal rocks that have experienced varying physical conditions within the continental crust. Granulites, therefore, record crucial evidence for reckoning the degree to which

* Corresponding author. Tel.: +54 358 4676198; fax: +54 358 4680280.
E-mail address: jotamendi@exa.unrc.edu.ar (J.E. Otamendi).

0024-4937/$ - see front matter © 2005 Elsevier B.V. All rights reserved.
doi:10.1016/j.lithos.2005.09.007

the crust is internally differentiated through intracrustal petrologic mechanisms. Lambert and Heier (1967) were among the first to show that compared to low pressure granulite-facies and amphibolite-facies terranes, medium to high pressure granulite terranes are depleted in those chemical elements that tend to be highly concentrated in felsic igneous rocks. Subsequent contributions identified the incongruent (peritectic) reactions that occur during partial melting at granulite-facies conditions and that, under intracrustal *P–T–X* conditions, these melting reactions need to be activated by the breakdown of hydrous minerals (Brown and Fyfe, 1970; Clemens and Wall, 1981; Thompson, 1982; Powell, 1983). Furthermore, since felsic melts at middle- to lower-crustal pressures may be capable of dissolving much more water than is released by the breakdown of hydrous reactants (Burnham, 1979), incongruent melting commonly gives rise to water-undersaturated melts and anhydrous residues. These inferences have been corroborated by subsequent experimental research (Vielzeuf and Holloway, 1989; Le Breton and Thompson, 1988; Patiño Douce and Johnston, 1991). Thus, it is envisaged that the widespread presence of felsic melts at upper crustal levels should be complemented by bodies of anhydrous melt-depleted granulites deep in the continental crust (Vielzeuf et al., 1990). Doubts have since been raised about the extent of separation of melts from residues during partial melting at lower crustal levels, essentially questioning if this process can lead to effective chemical differentiation within the continental crust (Rudnick and Presper, 1990). Consequently, whereas partial melting during metatexis and diatexis plays a key role in provoking geochemical differentiation during crustal reworking (Brown, 1994; Sawyer, 1998), the extraction of felsic melts from anhydrous granulite-facies residues may be an extreme and perhaps rarely reached condition (Clemens, 1990; Dostal et al., 2006).

Granulites include rocks that may have formed by a variety of processes, not all of which include melting and melt extraction. In fact, for granulite-facies rocks having similar mineral assemblages than those studied here, it was demonstrated that the Mg- and Al-rich bulk composition, together with high abundance of trace elements such as Zr, Ce and Th, was engendered by intense weathering of mafic volcanic material, and the subsequent evolution of the clay-rich sedimentary products in an environment evolving close to the Earth's surface (e.g. Moore and Waters, 1990). Following a similar line of reasoning but considering igneous material as precursors, a recently presented alternative asserts that fluid-mobile element depletions found in most granulites are a chemical feature inherited from their precursor (e.g. Rollinson and Tarney, 2005), as might be applicable to granulites derived from felsic igneous protoliths. Other studies have shown that some rocks with granulite-facies mineral assemblages can form as a result of subsolidus dehydration induced by a CO_2-rich fluid phase (Frost and Frost, 1987). Whereas important examples of granulites may have formed by such processes, many granulites show field and petrologic evidence that they were derived from crustal metasedimentary rocks and have features that strongly imply melt extraction, such as the absence of K-feldspar and the distinctive residual trace element signatures.

The granulites from the eastern Sierras Pampeanas are examples of granulites with mineralogical and geochemical features that are expected in a granulitic restite that lost nearly all the felsic melt component that was produced in it (see Otamendi and Patiño Douce, 2001). Hence, the primary aim of the present study is to present a model for the petrologic and geochemical evolution of granulites with these features. First, we use experimental results as major constraints to elucidate the major element variation that accompanied the generation of the restitic granulite, and then show how major element content that evolves toward the composition of a refractory residuum controlled the stability of minerals in the restitic assemblage. We then argue that both trace element and isotopic compositions of the intermediate Opx–Grt granulite cannot be simply explained by close-system fluid-absent melting. Finally, we demonstrate that some remarkable geochemical features of restitic granulites, such as Rb abundance and K/Rb ratio, are reasonably explained in terms of mineral stability.

2. Geological setting and field relations

The Rio Santa Rosa granulite body in the central eastern Sierras Pampeanas of Argentina occurs within a NW–SE trending package of Cambrian supracrustal rocks metamorphosed during an Early Cambrian (530 Ma) event (Rapela et al., 1998; Fig. 1A, inset). The Rio Santa Rosa granulite consists predominantly of refractory granulites, and is included as a thick lens in a package of melt-depleted migmatites (Fig. 1A). Four lithologies are identified within the Rio Santa Rosa granulite: garnet- and cordierite-dominated granulites, clinopyroxene-bearing metabasites, orthopyroxene- and garnet-granulites, and a mafic igneous suite chiefly composed of fine-grained gabbronorites and medium-grained orthopyroxenites.

The first two of these lithologies can be tied with confidence to protoliths in the supracrustal sequence. The metabasite occurs as discontinuous layers within the Grt–Crd granulite, which together retain structural evidences of an early deformation pre-dating the Cambrian thermal peak (e.g. Martino et al., 1994). At their

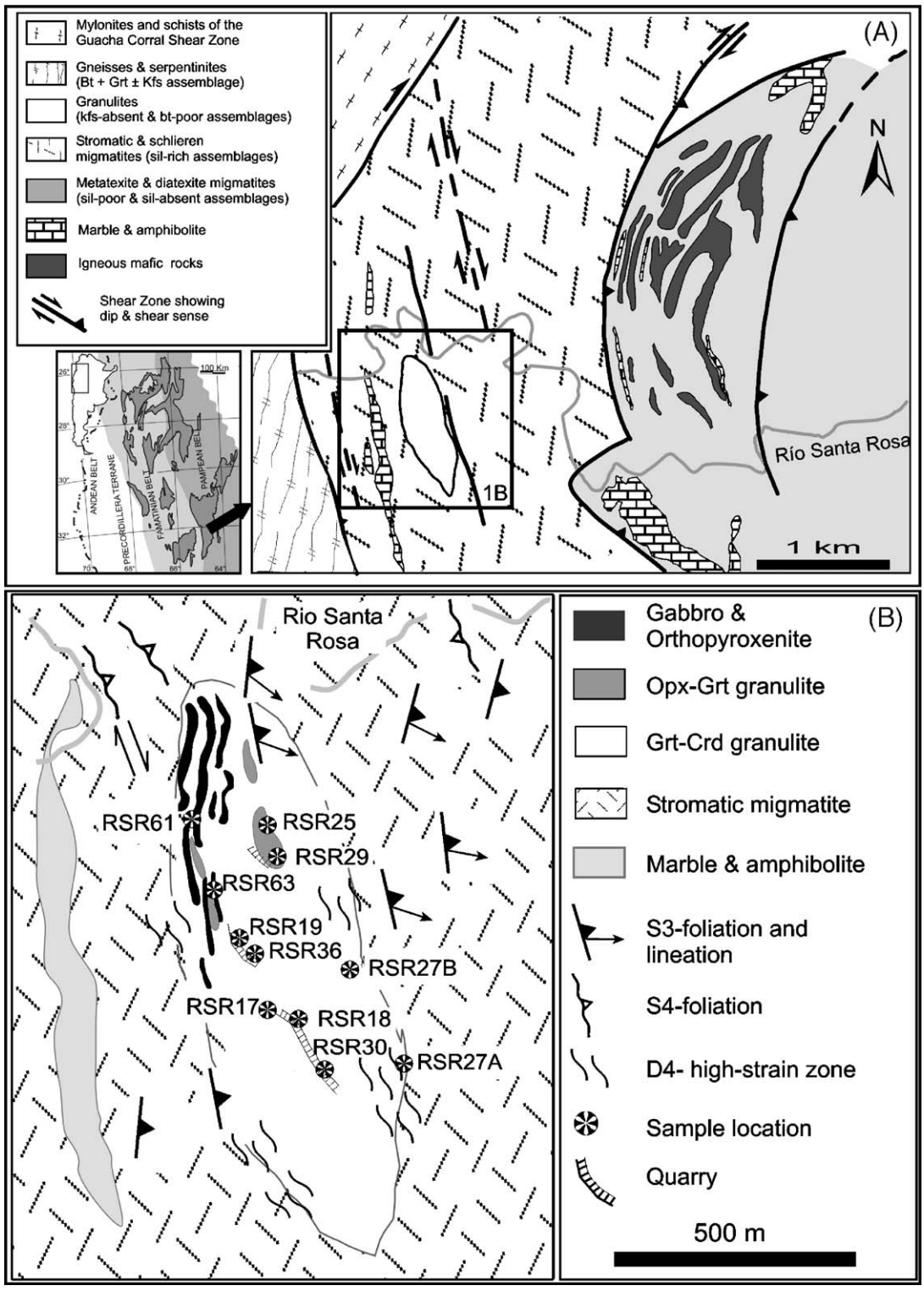

contact with Grt–Crd granulites, the metabasites show diffusion-controlled layering that was generated at peak conditions (Otamendi et al., 2005). Field relationships clearly prove that these rocks were interlayered by the time of the granulite-facies metamorphism.

The orthopyroxene- and garnet-granulites form lenses of up to 20 m long interleaved with the Grt–Crd granulites, and their contact is gradational over a few centimetres. The field characteristic that permits distinguishing these granulites in outcrop is a change of colour. Variations in mineral assemblages are otherwise difficult to discern on a hand specimen scale, and structural and textural features have imperceptible differences. The protolith for the Opx–Grt-granulites is less evident than those of other lithologies in the body, and its nature is discussed later in this work. Lastly, the rocks of the mafic igneous suite form an elongate N–S body intrusive into the western half of the Rio Santa Rosa granulite (Fig. 1B).

A relic gneissic fabric giving evidence for the early tectonic stage D_1 is locally found in the Sierra de Comechingones supracrustal sequence, within which the Rio Santa Rosa granulites occur. This crustal package experienced two major tectonic events D_2 and D_3, during which metamorphic conditions reached granulite-facies (Gordillo, 1984). *P–T* estimates for the metamorphic peak give pressures of 7.5 ± 0.5 kbar and a temperature range of 850–900 °C (Otamendi et al., 2005). Evidence from aluminous granulites supports the interpretation that a garnet-forming reactions followed by a garnet-consuming reactions developed as part of a single metamorphic cycle along a clockwise *P–T* path. Peak *P–T* results obtained in the orthopyroxene–garnet-granulites are similar to those of the aluminous granulites. D_2 comprises fold and fabric features interpreted to have formed in a stage that lasted from crustal thickening until the metamorphic peak. At the Rio Santa Rosa section D_2 deformation is almost completely reworked by subsequent events (Fig. 1B). The third phase of deformation (D_3) is a composite event consisting of at least two discrete fold- and fabric-forming phases. In migmatites at the eastern end of the granulite body, early stage D_3 structures tightly fold the stromatic D_2 fabric. Shearing with a top-to-WNW sense of movement at the west boundary of the granulite is associated with the D_3 stage (Martino et al., 1994). Late D_3 shear bands channeled anatectic cordierite-bearing leucosomes, suggesting that late anatexis and decompression were coeval with the D_3 episode. Progressive shearing under retrograde amphibolite- to greenschist-facies temperatures was accommodated in narrow belts during a D_4 deformation event. These shear zones led to exhumation of the high-grade sequence to upper crustal levels by the middle Palaeozoic.

3. Petrography and mineral chemistry

Petrographic descriptions and mineral chemistry data for the granulite rock types were presented elsewhere (Otamendi et al., 2005), however a brief description of petrographic features and summary of mineral composition are included below and in an electronic data repository for this article. Relevant differences in mineral compositions and assemblages among granulites, migmatites and regional gneisses were shown by Gordillo (1984), Martino et al. (1994) and Otamendi et al. (1999). Excluding textural relations preserved inside garnet porphyroblasts, the prograde metamorphic fabric of the granulites was thoroughly overprinted during melting and melt extraction. Linking texture and assemblage, it was deduced that rocks experienced D_2 fabric-forming deformational event under granulite-facies conditions (Martino et al., 1994). In agreement with this conclusion, the mineral assemblage defining the earliest foliation is refractory. Furthermore, this foliation is clearly distinguished from the effects of recrystallization and grain-size reduction under high-strain (D_3–D_4) deformations that occurred during post-peak stages. Retrogression of the anhydrous ferromagnesian minerals results in a hydrous lower temperature assemblage made up of anthophyllite, phlogopite and minor chlorite (Otamendi et al., 2005).

Grt–Crd granulites are characterized by a mineral shape-preferred orientation that is parallel to a crude discontinuous foliation. Granulites lack any vestige of well-defined metamorphic layering. The mineral assemblage Qtz + Pl + Grt + Crd + Ilm ± Ath extensively makes

Fig. 1. (A) Simplified geologic map of the northern-central Sierra de Comechingones showing that the Rio Santa Rosa granulite body is part of a supracrustal sequence that also contains unmelted gneisses, migmatites, marbles, amphibolites and ultramafic rocks. This lithologic package was intruded by mafic igneous rocks during and after the metamorphic peak. The inset on the lower left outlines the regional setting taken from Rapela et al. (1998) where crystalline blocks (dark grey) of the Sierras Pampeanas of central Argentina uplifted by the Andean tectonic are separated into two peri-Gondwana tectono-magmatic belts: the Cambrian–Pampean sequences in the east (grey) and the Ordovician–Famatinian sequences in the centre (light grey). (B) Geological sketch map of the Rio Santa Rosa granulite body showing sample locations and indicating the orientation of pervasive foliations.

Table 1

A. Major element bulk composition of Grt–Crd granulite, Opx–Grt granulite, and other spatially associated lithologies

Type	Grt–Crd granulite	Grt–Crd granulite	Grt–Crd granulite	Grt–Crd granulite	Grt–Crd granulite	Grt–Crd granulite	Grt–Crd granulite	Grt–Crd granulite
Sample	RSR-17	RSR-18	RSR-30	RSR-19A	RSR-50	RSR-36C	RSR-27A	RSR-27B
SiO_2	62.23	57.57	62.69	62.19	63.84	58.20	60.28	65.67
TiO_2	1.48	1.66	1.47	1.19	1.23	1.45	1.26	1.06
Al_2O_3	15.70	17.35	16.43	16.57	16.53	19.13	16.69	14.38
Fe2O3	10.52	12.94	10.85	10.97	8.63	11.21	9.09	9.08
MnO	0.24	0.27	0.21	0.25	0.21	0.20	0.18	0.20
MgO	4.47	6.21	4.29	4.42	4.57	5.72	3.29	3.22
CaO	2.50	1.87	2.43	2.67	2.26	1.93	4.16	3.71
Na_2O	1.15	0.82	1.04	1.30	1.11	0.92	2.27	2.13
K_2O	0.14	0.19	0.25	0.10	0.15	0.14	1.28	0.41
P_2O_5	0.02	0.03	0.02	0.02	0.02	0.02	0.03	0.02
LOI	0.90	0.78	0.61	0.30	0.36	1.02	0.68	0.37
Total	99.35	99.69	100.29	99.98	98.91	99.94	99.21	100.25

B. Trace element composition of Grt–Crd granulite, Opx–Grt granulite, and other spatially associated lithologies

Sample	RSR-17	RSR-18	RSR-30	RSR-19A	RSR-50	RSR-36C	RSR-27A	RSR-27B
XRF (ppm)								
V	129	105	135	173	166	189	127	125
Cr	201	244	224	122	n.a.	140	104	98
Co	47	47	46	143	n.a.	124	138	138
Ni	50	106	68	51	n.a.	52	158	42
Cu	5	5	5	2	n.a.	5	3	5
Zn	58	88	63	71	n.a.	84	55	63
Ba	12	25	28	31	21	31	165	39
Nb	5	7	5	10	7	11	10	10
Rb	5	6	7	3	5	6	51	7
Sr	88	60	91	109	76	73	141	138
Y	87	96	72	84	78	63	91	69
Zr	344	302	314	349	400	326	501	457
ICP-MS (ppm)								
Li	4	5	5	7	6	9	9	6
Sc	20	21	15	34	31	29	29	28
Ga	11	13	12	19	n.a.	22	24	16
Rb	3	6	4	3	n.a.	5	48	5
Nb	n.a.	n.a.	n.a.	9	n.a.	11	9	9
Cs	1.2	1.4	1.4	0.4	0.2	0.5	0.7	0.2
Ba	19	20	24	38	n.a.	45	168	45
La	8.6	12.7	8.8	14.9	15.3	13.8	16.8	11.7
Ce	23	22.7	20	28.7	29.6	26.3	31.9	21.1
Pr	2.9	2.9	2.2	3.6	3.1	3.3	3.9	2.5
Nd	11	10.7	8.4	13.2	11.8	13.1	14.7	9.3
Sm	2.1	2.7	2.1	3.4	2.9	3.4	3.0	2.2
Eu	0.6	0.5	0.6	1.0	0.8	0.8	1.3	1.1
Gd	4.4	5.1	3.9	7.0	6.0	7.2	5.1	4.5
Tb	1.2	1.3	1.0	1.8	1.7	1.7	1.4	1.2
Dy	10.3	11.2	8.4	13.9	12.6	12.1	12.7	10.0
Ho	2.5	2.7	2	3.4	3.0	2.8	3.6	2.6
Er	8.1	8.2	5.9	10.4	8.5	7.7	12.1	8.8
Tm	1.2	1.2	0.9	1.6	1.4	1.2	2.0	1.5
Yb	7.7	7.2	5.4	9.9	7.9	7.3	12.1	9.6
Lu	1.1	1	0.7	1.5	1.3	1.1	2.1	1.6
Pb	2.7	3.1	3.3	3.2	n.a.	4.5	6.7	3.6
Th	2.4	4.9	2.8	4.5	3.5	4.7	4.0	1.7

Rock types as in Table 1A. n.a. element not analysed; b.d.l. element abundance is below detection limit.

Grt–Opx–Crd	Opx–Grt granulite	Opx–Grt granulite	Opx–Grt granulite	Metabasite	Metabasite	Gabbronorite	Gabbronorite	Orthopyroxenite
RSR-36B	RSR-25B	RSR-25D	RSR-63	RSR-19B	RSR-36A	RSR-61	RSR-40	RSR-48
69.17	60.01	58.96	58.64	48.81	53.22	51.30	49.26	53.5
0.55	1.47	1.41	1.24	1.35	1.33	0.95	1.82	0.15
15.71	14.20	15.29	15.89	15.82	14.90	9.80	18.37	3.64
3.83	12.11	11.32	11.49	11.09	10.84	20.20	12.54	26.52
0.06	0.20	0.16	0.24	0.14	0.15	0.40	0.12	0.54
1.91	4.51	5.00	4.31	8.05	7.11	12.31	7.04	16.4
4.82	4.84	4.80	4.85	13.11	10.41	3.60	5.69	0.29
2.67	2.33	2.32	2.37	0.64	0.75	1.33	3.56	0.03
0.15	0.18	0.18	0.22	0.15	0.29	0.29	0.25	0.01
0.02	0.01	0.02	0.02	0.12	0.13	0.01	0.02	0.01
0.85	0.24	0.19	0.39	1.10	0.89	0.36	0.48	0.1
99.74	100.10	99.65	99.65	100.38	100.02	100.55	99.15	101.19

RSR-36B	RSR-25B	RSR-25D	RSR-63	RSR-19B	RSR-36A	RSR-61	RSR-40	RSR-48
73	224	222	193	248	277	187	264	142
52	152	143	138	371	258	255	170	264
144	93	99	98	59	63	66	54	86
31	34	66	33	189	88	108	175	246
22	16	36	13	35	56	93	n.a.	n.a.
36	118	130	109	102	98	220	145	269
52	42	41	35	70	43	32	49	b.d.l.
6	10	10	10	7	7	6	9	b.d.l.
4	3	3	2	3	4	3	2	b.d.l.
206	157	173	172	139	128	99	233	b.d.l.
14	14	35	62	32	29	12	1	10
60	609	634	544	94	95	38	23	19
3	8	8	7	6	7	6	n.a.	n.a.
7	26	25	28	42	39	27	15	64
15	22	23	19	23	21	15	31	19
2	2	2	1	2	3	3	2	b.d.l.
3	10	11	10	6	5	5	n.a.	n.a.
0.2	0.2	0.2	0.2	0.7	0.3	0.2	0.2	0.1
54	57	58	38	76	50	40	n.a.	n.a.
11.6	6.5	8.1	8.1	6.4	6.9	3.7	9.2	0.12
20.0	11.6	14.8	15.3	16.7	16.6	8.0	16	0.4
2.3	1.2	1.6	1.7	2.6	2.6	0.9	1.61	0.07
8.5	4.2	6.0	6.8	13.0	12.0	3.9	5.82	0.47
1.4	0.7	1.2	1.5	3.8	3.6	0.8	0.87	0.24
1.0	0.8	1.1	1.0	1.2	1.2	0.4	1.38	0.04
1.7	0.8	2.0	2.7	4.9	4.7	0.7	0.67	0.45
0.3	0.2	0.5	0.7	0.9	0.8	0.1	0.07	0.14
1.8	1.6	4.9	7.6	5.5	5.4	1.0	0.36	1.24
0.3	0.5	1.5	2.4	1.2	1.2	0.2	0.06	0.38
0.9	2.1	5.7	9.8	3.3	3.3	0.9	0.19	0.38
0.1	0.4	1.1	1.8	0.5	0.5	0.2	0.03	0.38
0.8	3.5	7.8	13.8	3.0	3.1	1.3	0.2	3.08
0.1	0.7	1.5	2.5	0.5	0.5	0.2	0.03	0.65
2.2	4.1	5.6	4.6	5.7	4.1	5.0	10	n.a.
1.0	0.3	0.8	1.1	1.0	0.9	2.7	0.15	0.07

up the aluminous granulite (abbreviations for minerals after Kretz, 1983). At the hand specimen scale the association Qtz+Pl+Crd forms irregularly shaped leucocratic domains. Garnet (X_{Mg}=Mg/Mg+Fe c. 0.40 in core) tends to concentrate in melanocratic layers, typically appearing as large subhedral porphyroblasts with embayed borders. Some garnets show poikiloblastic cores containing inclusions of Qtz±Sil±Ilm±Crd±Spl, and a rim zone almost devoid of inclusions. The limit between core and rim is marked by concentric rings of prismatic sillimanite, which outlines euhedral garnet faces. Cordierite (X_{Mg}=0.80–0.84) forms large subhedral crystals in garnet-rich domains but is amoeboid or sutured in quartzofeldspathic layers. Primary cordierite usually occurs as elongated crystals oriented parallel to the foliation and appears to be in textural equilibrium with garnet. Cordierite (X_{Mg}=0.85–0.89) also forms inclusion-free grains rimming garnets, and in recrystallized aggregates of Crd+Ath+Qtz+Ilm± Pl where it is fine-grained, sutured, and exhibits kinked twins. Plagioclase (An37 to An57, increasing rimward) occurs as large irregular grains with intracrystalline dislocations, and predictably is concentrated in leucocratic domains. Large crystals of anthophyllite (X_{Mg}=0.67–0.71) are associated with Crd-rich domains and form subhedral tabular grains. Anthophyllite also occurs as boudinaged aggregates of grains showing undulose extinction and mechanical twining. Fe–Ti oxides occur as needle- or bleb-like exsolution phases in anthophyllite. Phlogopite (X_{Mg}=0.63–0.73, TiO_2<2 wt.%) occurs as irregular interstitial laths that are included in the reabsorbed core of some garnets and adjacent to ferromagnesian phases, so it is interpreted that phlogopite crystallized at a post-D_2 stage.

Opx–Grt granulites commonly show a crudely developed textural and mineralogical foliation defined by the alternation of equigranular, pseudo-polygonal, mesocratic or leucocratic plagioclase- and quartz-dominated domains with inequigranular melanocratic orthopyroxene-dominated domains. The mineral assemblage is homogeneous and includes: quartz, plagioclase, orthopyroxene, garnet, and ilmenite and/or magnetite, with a variable proportion of biotite. Orthopyroxene (X_{Mg}=0.59–0.66, Al_2O_3=4.2–5.2 wt.%) forms subhedral prisms in coarse-grained, garnet-poor leucocratic domains, but subhedral or lobate medium-sized grains in domains having higher proportion of garnet. In garnet-rich domains, some orthopyroxene contain euhedral garnet inclusions. Garnet (X_{Mg}=0.31–0.38) occurs as subhedral porphyroblasts with embayed borders or as small polygonal crystals. Some garnet porphyroblasts are poikiloblastic with lobate quartz and subhedral plagioclase inclusions. Orthopyroxene and garnet grains are locally separated by an aggregate of plagioclase+-quartz. Plagioclase (An44 to An63) commonly forms subhedral grains in textural equilibrium with orthopyroxene and/or garnet. Plagioclase also locally occurs as lobate grains around reabsorbed garnet porphyroblasts, in which cases the plagioclase is slightly more calcic than the large plagioclase grains in the medium-grained matrix. In a few cases, plagioclase contains small inclusions of euhedral garnet.

Metabasites consist of clinopyroxene and plagioclase with lesser hornblende and rare quartz. A mineral shape-preferred orientation is displayed parallel to the compositionally defined foliation. These features certainly result from metamorphic segregation. In contrast, gabbronorites lack obvious mineral shape-preferred orientations and have apparent igneous textures. This notable characteristic argues for distinct origins for the metabasites and gabbronorites. Metabasites are interpreted as mafic "basaltic" rocks interlayered within the supracrustal sequence, which also contained the sedimentary precursor to aluminous granulites (e.g. Rapela et al., 1998), whereas gabbronorites occurs as tabular bodies that intruded granulites. The absence of chilled margins in the gabbronorites reveals that they were injected into the granulites while they were still at high temperature.

4. Geochemistry of Rio Santa Rosa granulites

4.1. Analytical procedure

Bulk rock chemical analyses (Table 1) were carried out on rocks representative of each lithologic type, and the results are discussed below along with the major element whole-rock composition of three Grt–Crd granulites previously reported by Otamendi and Patiño Douce (2001). Every sample consists of more than 5 kg of wholly fresh material collected from blasted faces in quarries. After crushing the whole sample, approximately 500 g of homogeneous pebble-sized material were pulverized within a tungsten-carbide grinding bowl. Major elements and selected trace elements (V, Cr, Co, Ni, Cu, Zn, Ba, Nb, Rb, Sr, Y, and Zr) were determined by X-ray fluorescence (XRF) at the University of Oviedo, Spain, using glass beads and pressed powder pellets, respectively. Typical precision of XRF technique is better than ±1.5% (relative). Major element analyses of the garnet–cordierite granulites obtained via XRF are consistent within their uncertainties with values previously determined via atomic absorption spectrometry (see Otamendi and Patiño Douce,

2001). Trace elements, including some of those analysed by XRF, were determined by inductively coupled plasma mass spectrometry (ICP-MS) at the University of Huelva, Spain. The average precision and accuracy for most of these elements fall in the range of 5–10%, and they were controlled by repeated analysis of SARM-1 (granite) and SARM-4 (norite) international standard rocks of the South African Bureau of Standards (de la Rosa et al., 2001). In the case of trace elements analysed by the two methods (XRF and ICP-MS), values determined by XRF are considered to be more accurate, so the XRF data were used to constrain the petrogenesis of rock. Isotopic analyses for Sr and Nd (Table 2) were performed at the University of Granada, Spain, using a Finningan MAT-262 mass spectrometer. Analytical procedure was identical to that described by Montero and Bea (1998). For this work, $^{87}Sr/^{86}Sr$ ratios were corrected for mass-fractionation by normalizing to $^{88}Sr/^{86}Sr=8.375209$. Repeated measurements of $^{87}Sr/^{86}Sr$ in the NBS-987 standard yield an average that is better than 0.0007% (2σ). A similar method was used for Nd isotope determinations. The normalization value for $^{143}Nd/^{144}Nd$ is $^{146}Nd/^{144}Nd=0.7219$. Measurements of the La Jolla standard yield a value of 0.511840 ± 0.003 which is better than 0.0014% (2σ) of the accepted value.

4.2. Major elements

Grt–Crd granulites have a fairly homogeneous major element compositions. Typically these granulites show a moderate range in SiO_2 contents (57–64 wt.%) and low alkalis ($K_2O<0.25$ wt.%, $Na_2O<1.3$ wt.%). Low alkali contents and moderate Al_2O_3 contents (15.5–17.4 wt.%) lead to strongly peraluminous compositions with an alumina saturation index [$ASI=Al_2O_3/(CaO+Na_2O+K_2O)$ molar] from 2.3 to 3.5. The molar ratio $Al_2O_3/FeO+MgO$ varies from 0.54 to 0.67, whereas the X_{Mg} ($X_{Mg}=MgO/MgO+FeO$) is between 0.44 and 0.50. Greater chemical diversity for the Grt–Crd granulites appears in samples located both in the eastern marginal zone (samples RSR27A and RSR27B, Table 1) and next to the metabasite (RSR36C). Compared to the typical Grt–Crd granulites, rocks in the eastern border have higher alkali and lime content, but lower X_{Mg} of around 0.41. These differences are consistent with a higher proportion of plagioclase, and with the less refractory character as suggested by the persistence of high-Ti biotite in the marginal granulites. The Grt–Crd granulite (RSR36C) sampled in the contact with metabasites (RSR36A) is slightly enriched in Al_2O_3, and shows lower SiO_2 content. This might reflect silica lost from the granulite towards the metabasite, however granulite still retains its aluminous and refractory composition (Otamendi et al., 2005).

Major element composition of the Opx–Grt granulites differs from that of the Grt–Crd granulites in having higher CaO abundances and a lesser enrichment of Na_2O contents (Table 1). Opx–Grt granulites are weakly peraluminous (ASI=1.1–1.2). However, their molar $Al_2O_3/FeO+MgO$ ratio (c. 0.55) as well as their X_{Mg} value (c. 0.45) are roughly similar to those of the Grt–Crd granulites. The CaO content seems to control the mineral assemblage that is able to coexist in the granulite types. This is explored using chemographic diagrams (Fig. 2). For granulites that have bulk rock composition showing a very low K_2O content, and neglecting the unconstrained effect of H_2O, the chemographic analyses can be treated in the system $NaO_{1/2}$–CaO–MgO–FeO–$AlO_{3/2}$–SiO_2 (Spear, 1993). Projection of mineral and whole-rock chemistry is performed from quartz and plagioclase having an anorthite-fixed composition into the CaO–MgO–FeO–$AlO_{3/2}$ tetrahedron (Fig. 2). It shows that the bulk composition of Opx–Grt granulites

Table 2
Sr and Nd isotope data for aluminous and intermediate granulites and gabbronites

Rock type sample	t (Ma)	Sr (ppm)	Rb (ppm)	$^{87}Sr/^{86}Sr$	$^{87}Sr/^{86}Sr(t)$	$\varepsilon Sr(t)$	Nd (ppm)	Sm (ppm)	$^{143}Nd/^{144}Nd$	$^{143}Nd/^{144}Nd(t)$	$\varepsilon Nd(t)$	TDM
Aluminous granulite												
RSR-50	530	76.0	5.3	0.708504	0.706981	41.48	11.80	2.90	0.51225	0.511734	−4.3	1.54
RSR-19A	530	109.5	2.8	0.709171	0.708607	64.58	13.22	3.41	0.51235	0.511809	−3.0	1.42
Intermediate granulite												
RSR-25B	530	156.7	2.5	0.706177	0.705821	25.01	4.20	0.74	0.512242	0.511874	−1.6	1.30
RSR-63	530	171.8	1.8	0.70824	0.708013	56.15	6.79	1.50	0.512245	0.511781	−3.4	1.42
Gabbronorite												
RSR-40	530	232.7	1.8	0.707235	0.707067	42.70	5.82	0.87	0.512205	0.511890	−1.3	1.32
RSR-61	530	98.5	3.3	0.705162	0.704427	5.21	3.91	0.85	0.512264	0.511809	−2.8	1.47

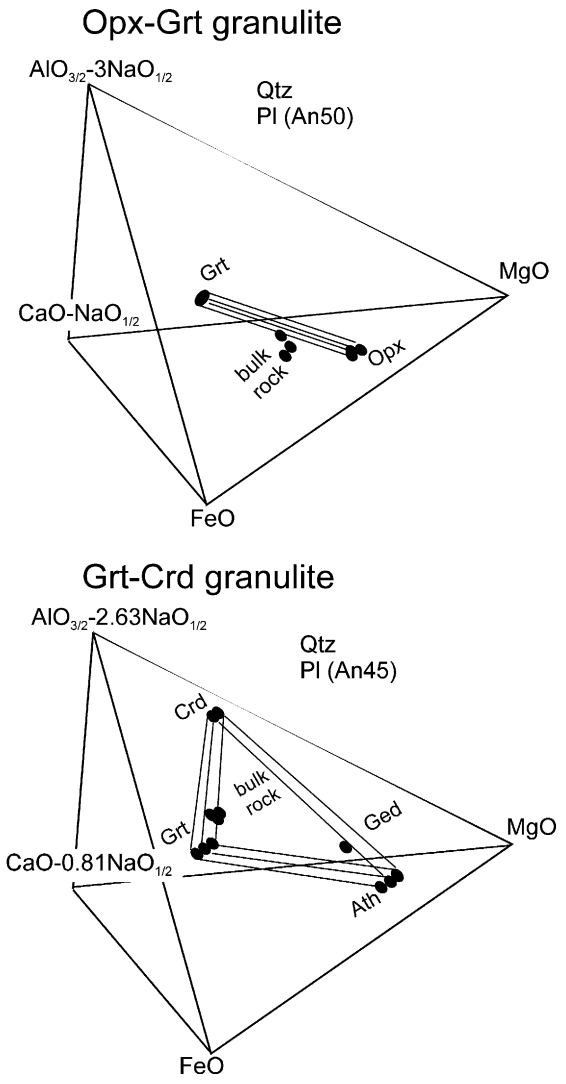

Fig. 2. ACFM tetrahedron showing the relative positions of minerals and bulk compositions of Opx–Grt granulites (upper diagram) and Grt–Crd granulites (lower diagram).

lies below but close to the garnet-orthopyroxene tie-line. Thus, under *P–T* conditions at which garnet and orthopyroxene coexist, cordierite crystallization in the Opx–Grt granulites is not possible because cordierite and bulk rock composition lie on opposite sides of the garnet–orthopyroxene tie-line. In contrast, the bulk rock chemistry of the Grt–Crd granulites lies along or slightly below the garnet–cordierite tie-line, consistent with a modal composition dominated by quartz, plagioclase, garnet, and cordierite. On the other hand, petrography gives ambiguous evidence for the presence of other ferromagnesian minerals (anthophyllite, gedrite, or eventually orthopyroxene) as primary phases in Grt–Crd granulites. Hence, the issue of whether orthoamphibole coexists at peak temperatures with garnet and cordierite is reserved for later discussion.

Metabasites, which are metamorphic rocks certainly derived from igneous precursors (e.g. Rapela et al., 1998), have major element composition resembling those of the tholeiitic basalts. Gabbronorites showing igneous-looking textures have major element chemistry unambiguously reflecting their mineral constitution. The concentration of Fe_2O_3 (as total Fe) and MgO is characteristically high and increases with increasing orthopyroxene modal proportion. The trend of CaO abundance is opposite to that of Fe_2O_3 and MgO, implying that the accumulation of the two major phases, orthopyroxene and plagioclase, competed to create geochemical diversity.

4.3. Trace elements

Compared with the average composition of the continental crust (e.g. Taylor and McLennan, 1985) Grt–Crd granulites are depleted in LILE (large-ion lithophile elements) and LREE (light rare earth elements). However, the extent to which these elements are depleted in Grt–Crd granulites is significantly variable. The abundance of Rb, Ba and K in the bulk crust is considerably higher (6 to 10 times) than in Grt–Crd granulites (Fig. 3), whereas average crust has an abundance of Sr, Cs, Th, and LREE (e.g. La–Sm) that is slightly higher (1.5 to 4 times) than those of the Grt–Crd granulites. Furthermore, Grt–Crd granulites have marked enrichments in both middle and heavy rare earth elements (MREE and HREE; Gd–Lu), in yttrium, and in high field strength elements that are essential structural component of accessory minerals (e.g. Ti and Zr). There is a decoupling in the relative abundance of transition metals (Fig. 3A). One subgroup (Cr, Sc, Co, Ni) is enriched in granulites relative to the crust, whereas other metals (V, Cu, Pb) have a similar or somewhat lower abundance in granulites than in the bulk crust. This suggests that the first subgroup of transition metals is incorporated by garnet (and oxides) with high effective partition coefficients (see Fig. 3B). If granulite chemistry is compared with the composition of the upper crust larger depletions in LILE and LREE would exist than those noted above (Fig. 3B). In contrast, Eu in granulites is close to that of the average upper crust, and the abundance of some metals (e.g. Ni, Cr, V, Ti, Sc and Cu not shown) is enriched in the Grt–Crd granulites relative to the upper continental crust.

All Grt–Crd granulites have roughly V-shaped chondrite-normalized REE pattern (Fig. 4A and B) with distinctive HREE enrichment ($HREE_N > 30$, subscript

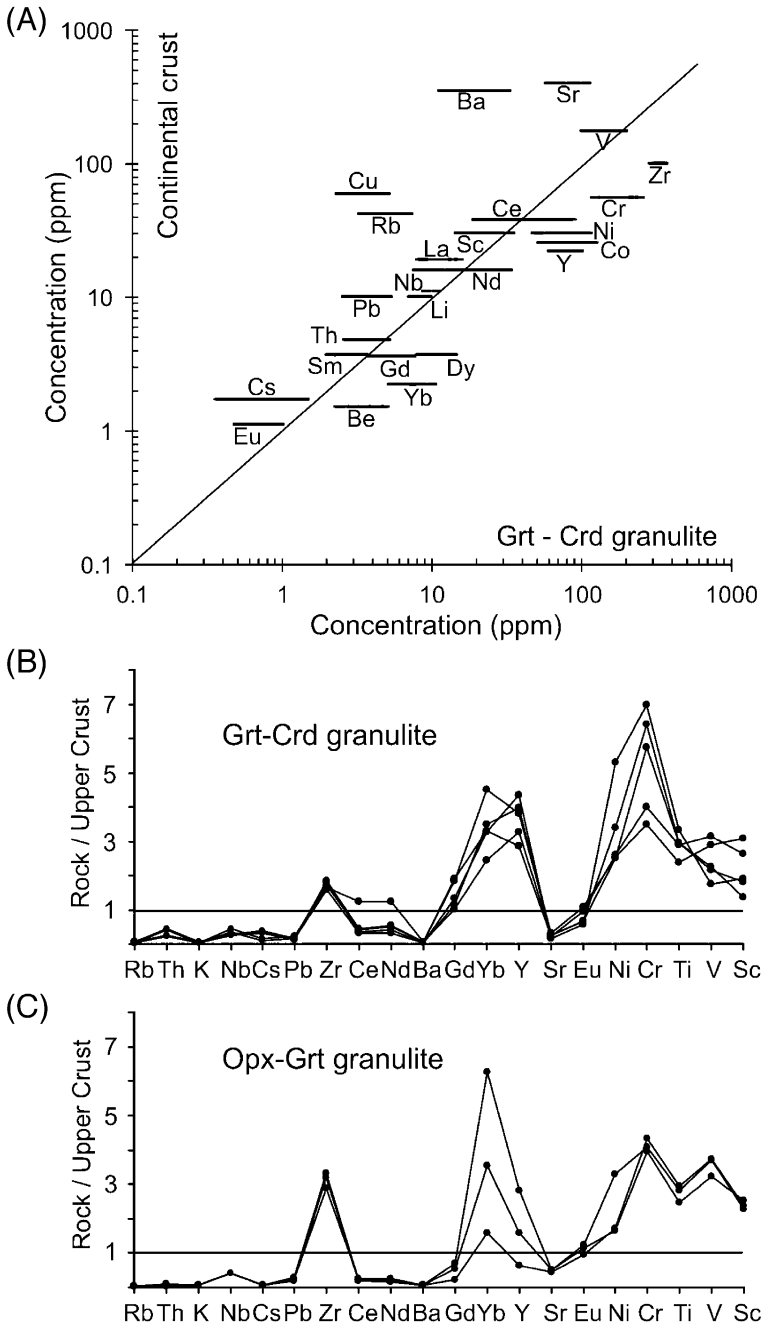

Fig. 3. (A) Comparison of trace element abundance in Grt–Crd granulites with the average of the bulk continental crust based on the andesite model of Taylor and McLennan (1985, their Table 3.3). (B and C) Trace element concentrations of Grt–Crd granulites (B) and Opx–Grt granulites (C) normalized to the chemical composition of the upper continental crust from Taylor and McLennan (1985). In these multi-element diagrams, the elements are ordered from left to right in a way that follows the decrease in the values of the upper crust/average crust element ratios.

N denotes chondrite-normalized values). The LREE contents ($La_N < 40$) is abnormally low for crustal rock and implies for the scarcity of LREE-rich accessory phases in these granulites. Typical Grt–Crd granulites, making up most of the granulite body, also have significant negative Eu anomalies (Eu/Eu* = 0.41–0.65) which arise from their low absolute Eu abundances rather than reflecting the enrichment in MREE (particularly of Gd that is used to estimate Eu*). The REE patterns also show that Eu is depleted at a similar extent

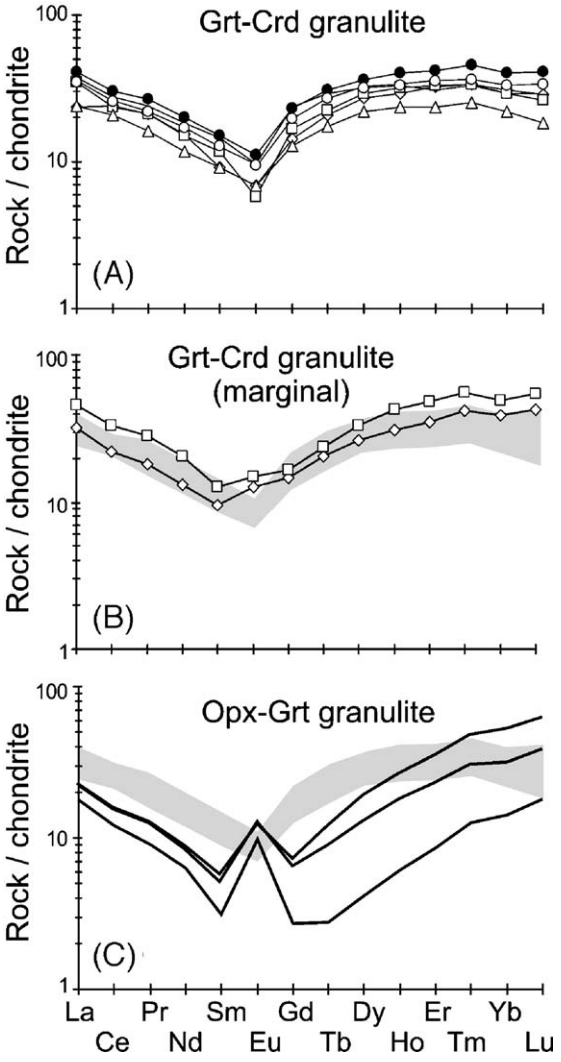

Fig. 4. REE pattern of granulites, normalized to the recommended chondrite value of Taylor and McLennan (1985). (A) Typical Grt–Crd granulites. (B) Grt–Crd granulites in the marginal zone of the granulite body. (C) Opx–Grt granulites. In diagrams (B) and (C) the field for typical Grt–Crd granulites is shown in grey.

as the LREE, which evidently indicates loss of Eu during granulite formation. Consistent with this, Grt–Crd granulites from the margin of the body, which according to petrography and major elements data are comparatively enriched in plagioclase, have no or even mildly positive Eu anomalies (Fig. 4B).

With the exception of few notable features, such as a high Yb/Y ratio and lower chromium content, Opx–Grt granulites display trace element patterns normalized to the upper continental crust roughly similar to those of the Grt–Crd granulites (Fig. 3C). The Opx–Grt granulites also have strong positive Eu anomalies (Eu/Eu* ~3, Fig. 4C), however, Eu absolute contents are not noticeably higher than those of Grt–Crd granulites. The positive Eu anomalies thus mirror the low contents of LREE and MREE in the Opx–Grt granulites. One other feature characteristic of REE pattern in these granulites is the steep increase from MREE to HREE (Gd_N/Yb_N ~0.2). Opx–Grt granulites contain both orthopyroxene and garnet, each of which is capable of producing fractionation between MREE and HREE. This unusual REE pattern shape is therefore attributed to the presence of these rock-forming minerals in variable modal proportions.

Metabasites have a primitive mantle-normalized pattern that is flat at 10× of the primitive mantle composition (Fig. 5A). This trace element signature differs slightly from that of a typical MORB (mid-ocean ridge basalt) in having higher concentrations (two to four times more than MORB) of lithophile elements (Rb,

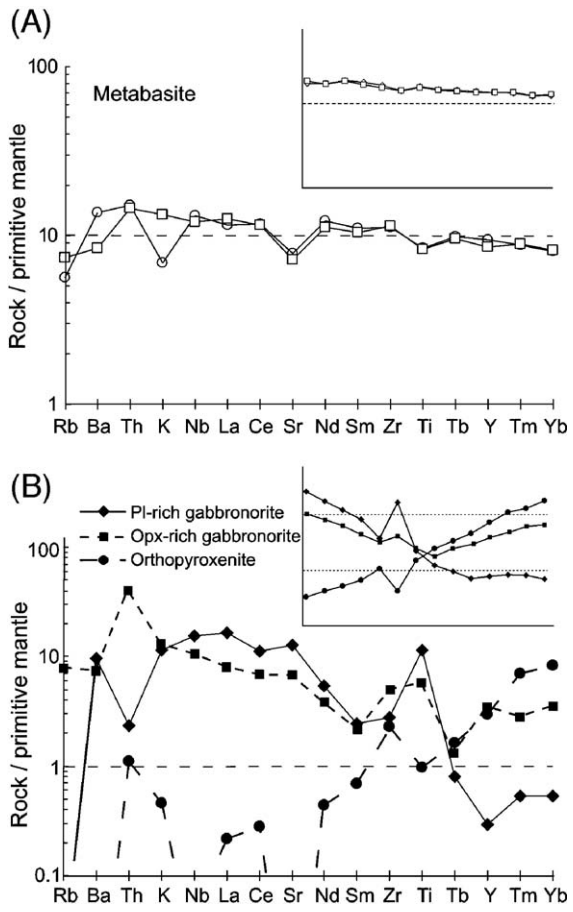

Fig. 5. Trace element concentrations of metabasites and gabbronorites/orthopyroxenite, normalized to primitive mantle composition of Taylor and McLennan (1985). (A) Multi-element diagram of metabasites; inset shows chondrite-normalized REE patterns. (B) Multi-element diagram of the mafic igneous suite; inset shows chondrite-normalized REE patterns.

Ba, Th, K). Except for a slight enrichment in LREE, the abundances of other REEs in metabasites are similar to that of typical MORB (Fig. 5A, inset).

Trace element abundance of gabbronorites could not be linked to the chemical signature of the parental magma as these mafic rocks are products of mineral accumulation (Fig. 5B). Except for the erratic abundance of Th, gabbronorites have relatively flat pattern for the incompatible lithophile elements at around 10× primitive mantle. The REE pattern of the gabbronorites displays a distinctive positive Eu anomaly (Fig. 5B, inset). However, the gabbronorite with the highest positive Eu anomaly has a fractionated REE pattern ($La_N/Yb_N=31$), whereas the other gabbronorite shows a moderate Eu anomaly with a roughly V-shaped REE profile. As enlightened by the REE pattern of the orthopyroxenite with a smooth positive slope, the differences in REE abundances between the two gabbronorites are simply one of the relative amounts of orthopyroxene and plagioclase making up them.

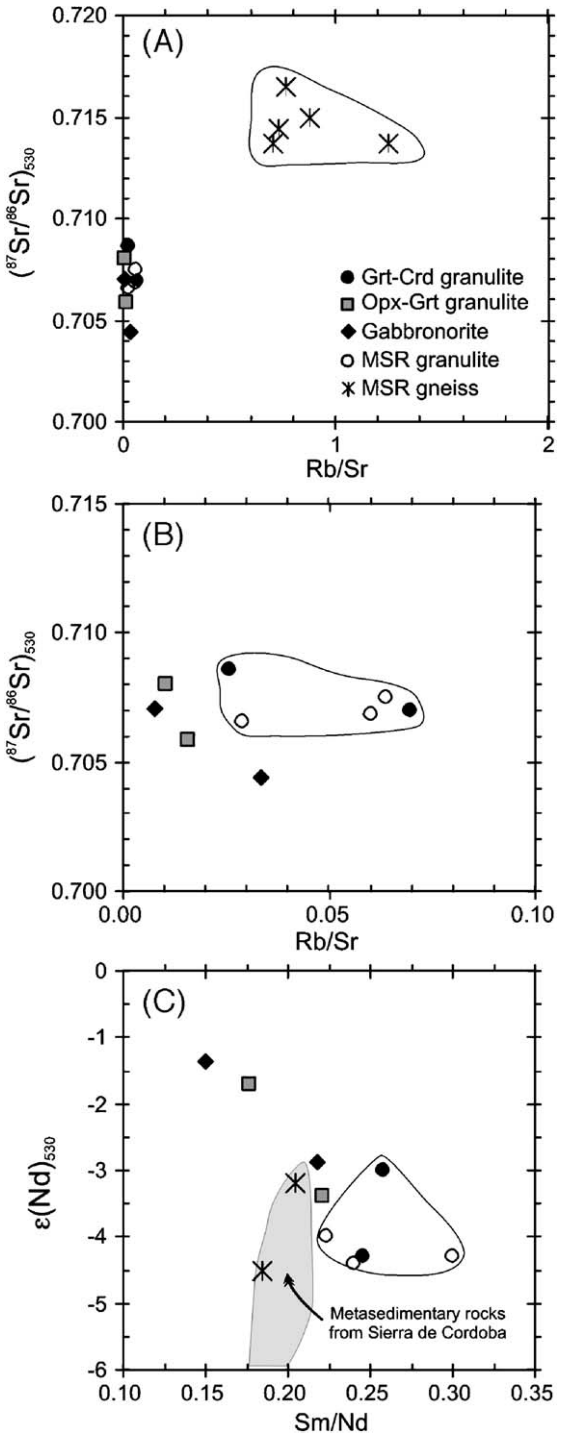

Fig. 6. (A) Initial Sr isotopic ratios at 530 Ma vs Rb/Sr ratio. 530 Ma is the most likely crystallization age for these rocks. Data for rocks from Santa Rosa Massif (MSR) reported by Rapela et al. (1998) are shown for comparison. MSR granulites are rocks sampled in the granulitic body studied here (see Fig 1), whereas MSR gneisses are unmelted gneisses and migmatites making up the same supracrustal package as the granulites. (B) Same as (A) but restriction to low Rb/Sr values to better show variations among the granulites and gabbronorites. (C) $\varepsilon_{Nd(530)}$ vs Sm/Nd ratio. A shaded field for metasedimentary rocks of the Lower Cambrian crystalline sequence from the Sierras de Cordoba (see Rapela et al., 1998) is shown for comparison. In diagrams (B) and (C) the circled field brackets by using all available data of the isotopic variation of aluminous granulites.

4.4. Sr- and Nd-isotope ratios

All Grt–Crd granulites have substantially lower Rb/Sr ratios than gneisses and migmatites from the same supracrustal sequences (Fig. 6A, see also Rapela et al., 1998), however, of even greater significance is that the values in $^{87}Sr/^{86}Sr(t)$ shown by Grt–Crd granulites are distinctively lower than those obtained for all other non-granulite metasedimentary rock from the same crustal package (Fig. 6A). Moreover note that there is an isotopic compositional gap between the initial $^{87}Sr/^{86}Sr$ ratios (<0.708) of the aluminous granulites and those of the regional high-grade gneisses (>0.713). Opx–Grt granulites have $^{87}Sr/^{86}Sr(t)$ ratios falling in the range of Grt–Crd granulites (Fig. 6B), but one of the Opx–Grt granulites (RSR25B) exhibits an $\varepsilon Nd=-1.6$ that is significantly more radiogenic than those of the rest of the granulites. When all data from the studied body are considered together, the two analysed gabbronorites have a slightly less radiogenic isotopic signature than aluminous and intermediate granulites, however, the $^{87}Sr/^{86}Sr(t)>0.704$ and $\epsilon Nd<-1.3$ ratios of the gabbronorites (Fig. 6C) are considerably outside the mantle array, indicating they must have experienced contamination with crustal rocks (Faure, 1986).

5. Discussion

5.1. Application of experimental results to interpret the genesis of Rio Santa Rosa granulites

Otamendi and Patiño Douce (2001) stated that the simplest way to produce the mineral assemblage of the Rio Santa Rosa aluminous granulites is residual rocks after melt loss via the general reaction:

$$\mathrm{Qtz} + \mathrm{Pl1} + \mathrm{Bt} \pm \mathrm{Sil} \pm \mathrm{H_2O} \rightarrow \mathrm{melt}(+\mathrm{H_2O}) + \mathrm{Grt} + \mathrm{Pl2} + \mathrm{Ilm} \pm \mathrm{Crd} \pm \mathrm{Opx} \pm \mathrm{Oam} \quad (\mathrm{R1})$$

This idea will be tested below by integrating bulk rock chemistry with mineralogical data and considering experimental constraints.

The results of melting experiments are used below to constrain the composition of the precursor to the studied granulites, and to identify chemical changes experienced by the aluminous granulites during formation and segregation of partial melts. Projection from major oxides (SiO_2, Al_2O_3, FeO total, MgO, CaO, Na_2O, K_2O, H_2O) into the system AKF (Fig. 7A) provides a suitable compositional space to display the relationships among starting material and run products in experiments, and for comparing the studied rocks with experimentally determined phase relations. Two starting materials are considered here, representing extremes in composition within the group of siliciclastic supracrustal rocks: a strongly aluminous plagioclase-poor metapelite (HQ-36, Patiño Douce and Johnston, 1991), and a synthetic biotite-rich gneiss (SBG, Patiño Douce and Beard, 1995). These materials were experimentally melted under both fluid-absent and fluid-fluxed conditions (Patiño Douce, 1996).

A notable difference between these materials is that the metapelite composition allows the stable coexistence of Grt+Bt+Sil at amphibolite-facies temperatures (Fig. 7B), whereas the low effective Al_2O_3 component of the biotite-rich gneiss (lower than that of biotite) hampers the crystallization of more than one

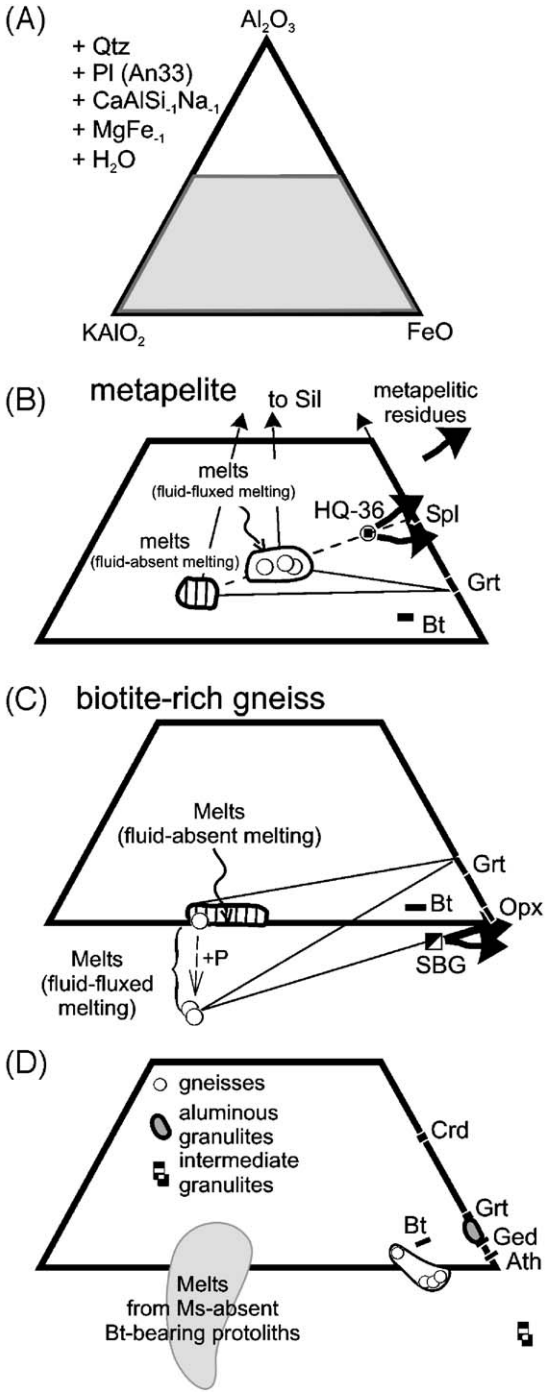

Fig. 7. (A) Part of the AKF diagram selected after condensing the SiO_2–Al_2O_3–FeO*–MgO–CaO–Na_2O–K_2O–H_2O system by projecting from appropriate phase components and exchange vectors into Al_2O_3–$KAlO_2$–FeO space. The shaded quadrilateral section is used in (B) through (D). (B) Projected composition of metapelite HQ-36 melted under both water-absent and water fluxed conditions (Patiño Douce and Johnston, 1991; Patiño Douce, 1996). Tie-lines connect peritectic products (Grt, Spl) and aluminosilicate (Sil) that remain as a stable phase until biotite (Bt) is exhausted. If melt is extracted, the bulk composition of the residue changes as indicated by the arrows. (C) Projection of the phase relationships during melting of biotite-rich gneiss (Patiño Douce and Beard, 1995). The dominant peritectic product is orthopyroxene (Opx) with garnet (Grt) present at low melting degrees. Note that the compositions of fluid-fluxed melts (empty circles) are less aluminous with increasing pressure. (D) Projection of mineral and bulk rock compositions of granulites. The composition of gneisses (unmelted metamorphic products) and granites (extracted melt) from the Sierra de Comechingones is taken from Otamendi and Patiño Douce (2001) and unpublished data.

aluminous ferromagnesian phase at any temperature (Fig. 7C). The relevance of these phase relations is that protoliths with compositions overlapping or below the projection of biotite compositional fields would contain at most only minor amounts of strongly peraluminous phases such as muscovite and sillimanite. Thus, melting reactions will involve biotite, plagioclase and quartz as reactant phases. The experimentally defined phase relations at crustal pressures (6–10 kbar) demonstrate that the metapelitic granulites are Al_2SiO_5-saturated residues left after extraction of strongly peraluminous melts (Patiño Douce and Johnston, 1991; see Fig. 7B). In contrast, orthopyroxene should be the dominant ferromagnesian phase in granulites derived from biotite-rich material (Fig. 7C).

In terms of bulk composition, the studied Grt–Crd granulites represent an intermediate case (Fig. 7D), since they have a composition projecting on the Al_2O_3–FeO side of the AKF diagram, with an Al_2O_3 component lower than garnet but similar to or slightly higher than biotite. The position of Grt–Crd granulites in the AKF diagram indicates they are neither a metapelite nor an Al_2O_3-poor greywacke, but a weakly aluminous residual composition (Fig. 7D). The lack of $KAlO_2$ component in the projected compositions is additional evidence suggesting that the studied granulites are residues formed after extensive melting and efficient melt extraction (Fig. 7B, C, and D). The regional non-granulitic gneisses which make up most of the terrane hosting the Rio Santa Rosa granulites bear chemical and mineralogical features compatible with the supposition of being parental rocks to the Grt–Crd granulites. Almost all gneisses, which are

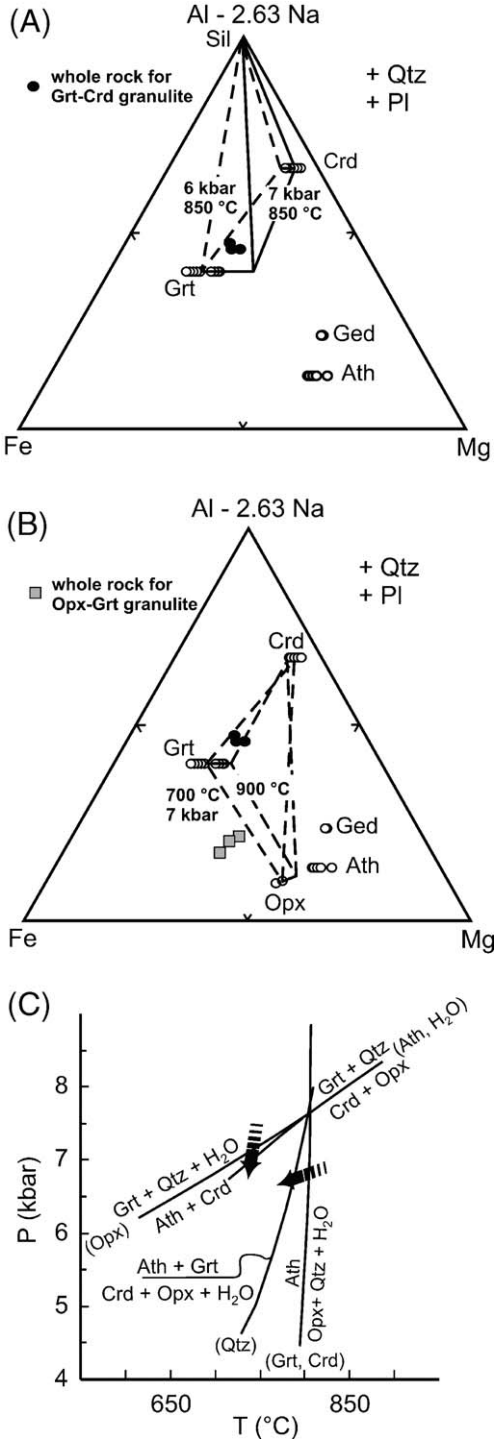

Fig. 8. (A) Projection of minerals (empty circles) and whole-rock compositions of granulites after condensing the SiO_2–Al_2O_3–FeO*–MgO–CaO–Na_2O system into the AFM space. Tie-lines join the position of Grt–Crd coexisting at a fixed P–T condition of interest. The X_{Mg} (=Mg/Mg+Fe) ratio of Grt and Crd in mutual equilibrium at a fixed P–T was estimated with the reaction Grt+Sil+Qtz↔Crd. It was sought that the reaction computed for phase components of the two subsystems FAS and MAS yields the following complementary result $X_{Mg}=1-X_{Fe}$ in garnet and cordierite. Thermodynamic data were taken from Berman (1988) and Berman and Aranovich (1996), however both minerals garnet and cordierite were considered ideal solid-solutions. (B) Theoretical Mg/Fe ratios of orthopyroxene coexisting in equilibrium with garnet and cordierite at selected T values of 700 and 900 °C, and a fixed P of 7 kbar. A simple constraint was used to get the coexisting X_{Mg} values in the three ferromagnesian phases. At the fixed P–T the three Fe–Mg exchanges that result from combining each phase with the other two must yield the same X_{Mg} ratios for each phase. The abundance of Al in Opx was assumed to be that in equilibrium with garnet at the fixed T. (C) P–T diagram illustrating alternative processes that may produce anthophyllite in a subsolidus assemblage having the mineral assemblage and bulk composition of the Grt–Crd granulites. This partial grid in the CaO–MgO–FeO–Al_2O_3–SiO_2–H_2O system was constructed for an assemblage Grt+Opx+Crd+Ath+Qtz+H_2O, which cannot be proven to be stable in the studied rocks, so that ideal mineral compositions were extracted from AFM relations.

interpreted as being derived from weakly aluminous quartz-rich greywacke-like sedimentary rocks (Otamendi and Patiño Douce, 2001) have biotite as the only hydrous prograde phase. These considerations support the idea that the aluminous granulites were derived from protoliths similar to those of the regional gneisses, and that the chemical trends experienced by granulites during melt extraction match those observed in residues in experimental studies. In contrast, the lower Al_2O_3 component in the Opx–Grt intermediate granulites is lower than expected for a residuum derived from regional gneisses, suggesting these granulites were derived from other protoliths.

The transition from gneisses to aluminous granulites involves additional chemical changes that cannot be effectively portrayed in the AKF projection. Major element compositions show that melting led to depletions in Na_2O as well as K_2O in the residual Grt–Crd granulites. Depletion of K_2O could have been caused by biotite breakdown, a process that advanced to complete consumption of prograde biotite in some rocks. Compared to the regional gneisses, granulites are depleted in Na_2O but enriched in CaO, indicating a decoupling of Na_2O and CaO during melting even though both major oxides are controlled by plagioclase. This implies that residual plagioclase became more anorthite rich rather than be consumed by the melting reaction (R1). The divergent behaviour of biotite and plagioclase is consistent with melting under fluid-absent conditions as the contribution of biotite as a reactant increases with decreasing water activity in the rock or coexisting separated fluid phase (Conrad et al., 1988; Patiño Douce, 1996).

5.2. Coexistence and relative stability of residual phases in Rio Santa Rosa granulites

The previous discussions recognized that the bulk compositions of the granulites evolved as a consequence of partial melting and melt segregation. Therefore it is important to consider how changes of the granulite composition affect the relative stability of the residual phase assemblage. It is noted that, omitting Ti-bearing oxides, most of the chemical variability among granulites may be accounted for in the SiO_2–Al_2O_3–FeO–MgO–CaO–Na_2O system, given that K_2O and H_2O were removed by the melt phase. A two-dimensional projection (AFM) derived from the 3D compositional space presented in Fig. 2 (Fig. 8A and B) permits a simpler graphical assessment of the effect of bulk composition on phase assemblages. This projection does not change the relative position of phases and bulk rock because, within the tetrahedral CaO–MgO–FeO–$AlO_{2/3}$ space, most of the phases lie close to MgO–FeO–$AlO_{3/2}$ plane, making the projection of mineral onto this plane from CaO apex rather short.

The bulk chemistry of Grt–Crd granulites lies inside the tie-lines linking garnet and cordierite equilibrated between 700 and 900 °C (Fig. 8A). During melt extraction the bulk composition of the granulite would have moved into the compositional field bounded by Grt–Crd tie-lines, both sillimanite and orthopyroxene would have reacted out. This may explain why sillimanite was consumed whereas orthopyroxene seems to have not crystallized during the consolidation of the granulite. It is an important insight since experimental studies suggest that if sillimanite is exhausted during partial melting by reaction (R1), orthopyroxene should be produced (Vielzeuf and Montel, 1994; Patiño Douce and Beard, 1995). If true, this would imply that either sillimanite was present throughout the melting stage, or orthopyroxene crystallized in the original residual assemblage and then became completely retrogressed to orthoamphibole (Fig. 8B). There is textural evidence for the presence of sillimanite in the pre-melting mineral assemblages of Grt–Crd granulites (Otamendi et al., 2005). However, there is no evidence indicating that sillimanite survived the melting process, and petrographic features indicate that the opposite case is most likely. The presence of early sillimanite requires that bulk rock lies above the garnet–cordierite tie-line, or that these lines were disconnected (Fig. 8A). The first possibility, that the unmelted precursors had a bulk composition closer to the Al apex in the AFM space than the studied aluminous granulites, is refuted by two observations. First, the index of aluminosity increases in parallel with the refractory character of the rocks, and granulites are the most extreme residual rock in the sequence of Sierra de Comechingones (Otamendi and Patiño Douce, 2001). Second, extraction of anatectic melts results in Na depletion of the bulk residue, shifting the projection of the residual rocks towards the Al–Na apex in the AFM diagram, so that the residue towards the Al (–Na) in the AFM diagram, requiring the residuum to be closer to the Al apex than its unmelted precursor.

A more plausible explanation for the early presence of sillimanite is that this mineral crystallized preceding the onset of cordierite stability, a possibility which is consistent with phase relationships (Fig. 8A) and textural assemblages found in the migmatites outcropping around the Grt–Crd granulites (Otamendi et al., 1999). With sillimanite present in the phase assemblage at an early granulite-facies metamorphic stage, the reaction (R1) could have been the chief mechanism for forming

both garnet and cordierite as melting progressed. However, orthopyroxene could have not grown as a peritectic phase because when sillimanite was totally consumed, the residual granulite had a bulk composition between garnet and cordierite in AFM space, and *P–T* conditions would allow the mutual coexistence of these two minerals (Fig. 8A). A completely different situation occur for the Opx–Grt granulites as their whole-rock composition plots well below Opx–Grt tie-lines (Fig. 8B), allowing Opx to crystallize when temperature rises into the Opx–Grt stability field.

Further insight into the early presence of orthopyroxene in Grt–Crd granulites requires consideration of the origin of orthoamphiboles. Grt–Crd granulites have variable modal proportions of orthoamphibole (up to ca. 18% modal). Most orthoamphiboles have a limited range in the anthophyllite end-member (0.67–0.72), whereas their Al_2O_3 contents vary from 2 to 6 wt.%. In a single specimen, Al-poor anthophyllite coexists with an Al-rich gedrite that has almost the same Mg-number (Fig. 8A). Orthoamphibole tends to occur spatially associated with cordierite, and is systematically involved in post-crystallization deformation bands, however there are few other compelling textural relations to guide interpretation of its origin. Experiments show that anthophyllite does not coexist in equilibrium with felsic melt at any P–T–X_{H_2O} condition, indicating it must be a subsolidus phase. Gedrite can be stabilized as a peritectic phase during partial melting of greywackes under fluid-present conditions (Conrad et al., 1988) and the gedrite stability field enlarges with increasing H_2O fraction in the fluid, however at relatively low temperatures (<825 °C). The possibility that anthophyllite, the most abundant orthoamphibole, grew by breakdown of gedrite is difficult to justify because crystallization of sufficient gedrite as a peritectic phase would conflict with the water-deficient conditions required for biotite exhaustion. Alternatively, anthophyllite could be produced by hydrous retrogression reactions involving either orthopyroxene and quartz or garnet and quartz (Fig. 8C). No vestiges of primary orthopyroxene have been found in the aluminous granulites, disfavoring the first possibility. The hydrous retrogressive reaction of garnet and quartz is catalyzed by decompression and produces anthophyllite and cordierite, features which agree with independent evidence that the granulites experienced decompression at high temperatures and that anthophyllite is commonly texturally associated with cordierite (Otamendi et al., 2005). We therefore find more likely that anthophyllite crystallization was catalyzed by the influx of fluids after the consolidation of the granulite assemblage.

5.3. Origin of Opx–Grt intermediate granulite within the Grt–Crd aluminous granulite

Opx–Grt granulites are usually interpreted as residues left after extended melting via the reaction:

$$\mathrm{Qtz} + \mathrm{Bt} + \mathrm{Pl} \rightarrow \mathrm{melt} + \mathrm{Opx} + \mathrm{Grt} + \mathrm{Ti\text{-}oxide} \pm \mathrm{Crd} \pm \mathrm{Kfs} \quad (\mathrm{R2})$$

which has been experimentally proved (Vielzeuf and Montel, 1994; Patiño Douce and Beard, 1995; Stevens et al., 1997). However, the Opx–Grt granulites studied here present some characteristics that conflict with the idea that they are the result of only melting and melt extraction process. Most notably, it is difficult to explain the enrichment in Sr and the REE patterns with a marked Eu positive anomaly by invoking only partial melting (e.g. (R2)), as plagioclase is a reactant phase. Excluding fluid-absent melting (R2), two processes may account for Opx–Grt granulite formation: subsolidus dehydration (Frost and Frost, 1987) and the reaction of mafic melts with metamorphic rocks at high temperatures (Patiño Douce, 1995). Dehydration is expected to be the dominant mechanism when the formation of granulite occurs under a distinctive fluid regime characterized by low H_2O activity (Harlov and Förster, 2002). The presence of a H_2O-poor fluid during granulite-facies metamorphism can be evaluated through the study of mineral fluid inclusions, however here we use the stability of K-feldspar as a criterion. This is justified because the subsolidus dehydration of a biotite- or hornblende-bearing assemblage inexorably forms K-feldspar as a product (Harlov and Förster, 2002), and K-feldspar may be either a solid peritectic product of partial melting or a component of the melt (Vielzeuf and Montel, 1994; Patiño Douce and Beard, 1995). The lack of K-feldspar in the studied granulites therefore makes it difficult to invoke dehydration as a causative mechanism, even though it cannot be absolutely ruled out with the available data.

The remaining mechanism for producing Opx–Grt granulites, by reaction of mafic magmas with aluminous granulites, is generally consistent with field evidence since a close spatial relationship is observed between mafic igneous rocks and Opx–Grt granulites. This mechanism is further evaluated using geochemical criteria. It should be noted first that it is difficult to determine the parental composition of the mafic magma since all gabbronorites show petrographic and geochemical evidence for having experienced mineral accumulation processes. However, these cumulates chiefly involve crystal accumulation of orthopyroxene

and/or plagioclase, and the co-variation of diagnostic major elements shows that the few sampled mafic rocks lie close to a line connecting orthopyroxene and plagioclase (Fig. 9A). By examining the covariations of major elements that are essential components and trace elements behaving compatibly in these phases, we are able to constrain the petrologic mechanism likely to have formed the Opx–Grt granulites.

The simplest case is for Sr, which increases with increasing Ca and thus reflects primary control by plagioclase (Fig. 9B). The higher Sr content in Opx–Grt granulites relative to other studied granulites cannot be consistently explained by progressive melt extraction, as the geochemical diversity observed in aluminous granulites shows that increasingly refractory the rocks have less Sr. Alternatively, if Opx–Grt granulites contain a mafic igneous component now represented by orthopyroxene, the behaviour of Sr should covary with trace elements controlled by orthopyroxene. In theory, there is no trace element that is strongly compatible solely in orthopyroxene. In practice, the bulk composition of the orthopyroxenite reveals that a few transition metals (Zn and Cr) are strongly enriched in this rock type and therefore are potentially controlled by ortho-

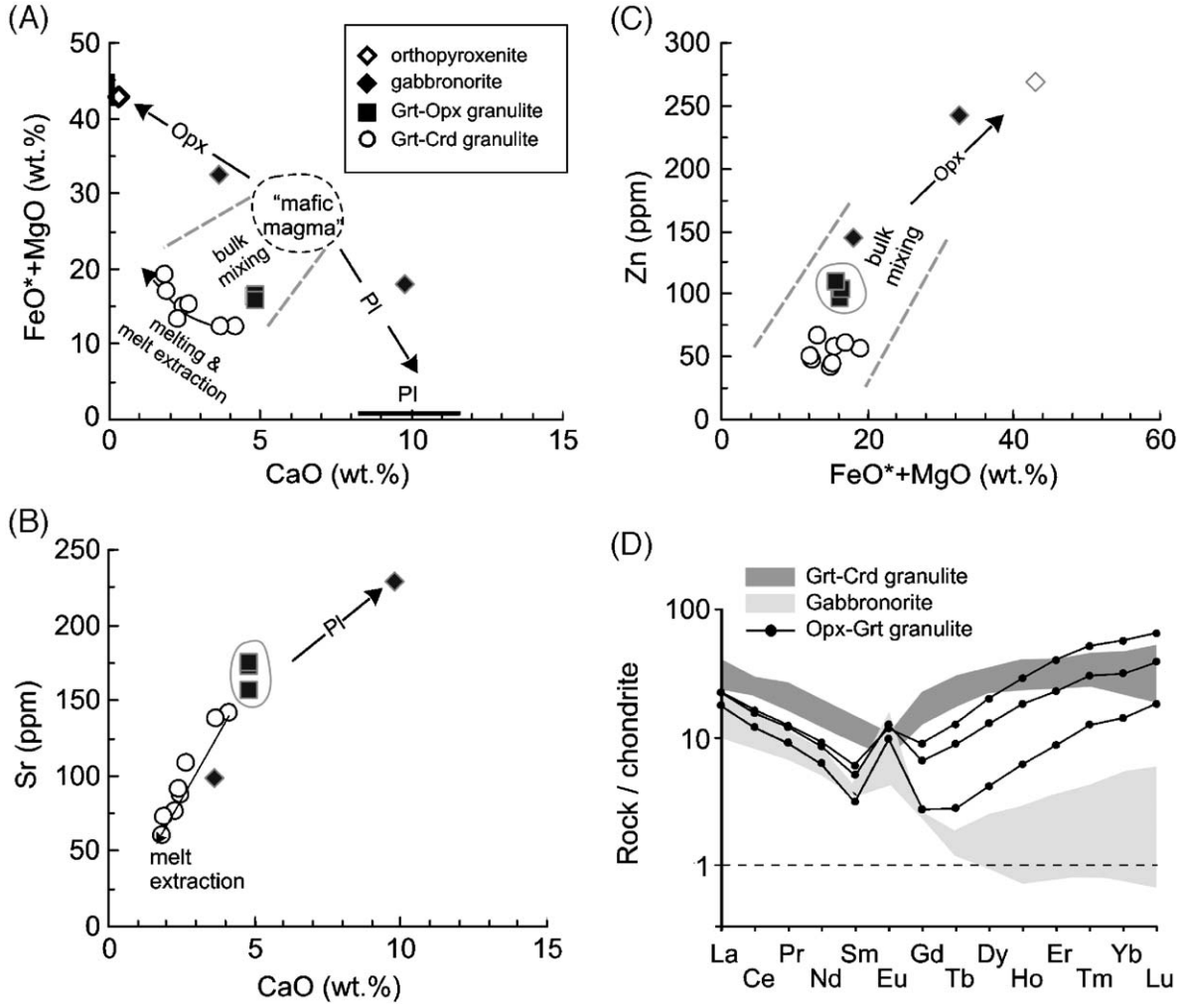

Fig. 9. Major and trace element abundance in the Opx–Grt granulites relative to Grt–Crd granulites and mafic igneous rocks. (A) Fe+Mg vs Ca plot showing the effects of cumulate formation dominated by either Opx or Pl in the mafic suite, the most likely compositional field of the parental mafic magma, and the chemical evolutionary trend followed by Grt–Crd granulites during melt extraction. (B) Sr vs Ca plot displays the behaviour of Sr, which is partitioned into Pl. Sr experiences enrichment in Pl-rich igneous rocks, however suffers depletion during melt extraction in aluminous granulites. The high abundance of Sr in the Opx–Grt granulites implies that Pl was a stable phase during their formation. (C) Zn vs Fe+Mg plot empirically shows that Zn is strongly partitioned into Opx and that Opx–Grt granulites have compositions that are intermediate between the aluminous granulites and mafic rocks. (D) Comparison of REE patterns of Opx–Grt granulites with fields for the REE patterns of gabbronorites and Grt–Crd granulites.

pyroxene. Since Cr can also be controlled by garnet and a small proportion of garnet is often present in orthopyroxenites, Zn is the best candidate to reflect the presence of igneous orthopyroxene (Fig. 9C). The abundance of Zn in Opx–Grt granulites is almost twice that of the other studied granulites. This feature cannot be ascribed to the process of restite formation, as peritectic minerals generated during partial melting are incapable of incorporating significant amount of Zn in their structures (see Otamendi and Patiño Douce, 2001). Furthermore, we have not found any pre-metamorphic sedimentary protolith in the region that is abnormally enriched in Zn. Therefore the simplest explanation of high Zn abundances in Opx–Grt granulites is to attribute it to a contribution from mafic magmas.

A high Yb/Y ratio is another relevant feature distinguishing Opx–Grt granulites from Grt–Crd granulites (Fig. 3B and C). Independently of the causal process, during the generation of the studied granulites the behaviour of both Yb and Y is governed by garnet (Otamendi et al., 2002). Furthermore, garnet would not only incorporate Yb and Y with very high partition coefficients, but also would tend to capture more Yb than Y (e.g. Rollinson, 1993). The conflicting aspect is that Opx–Grt granulites have fewer proportions of garnet but higher Yb/Y ratios than Grt–Crd granulites. An explanation to this discrepancy may be that Opx–Grt granulites contain an igneous mafic component in them, as mafic rocks, and in particular the orthopyroxenite, are the rocks having the highest Yb/Y ratios of the studied body (Fig. 5B). The REE patterns of the Opx–Grt granulites further support the idea that they are hybrid products formed by reaction of mafic magmas and aluminous granulites. Any attempt to petrologically model this process is hampered by the fact that the exact composition of the parental mafic magma is uncertain. However, in a qualitative way, the REE pattern of Opx–Grt granulites may be reasonably reproduced after combining the depletion of LREE and the positive Eu anomaly of mafic rocks with the strong enrichment of the HREE of the aluminous granulites (Fig. 9D). Further evidence for the origin of Opx–Grt is presented in the following section.

5.4. Sr- and Nd-isotopic differences between granulites and other stratigraphically related metasedimentary rocks

A notable feature of the studied granulites is that their $^{87}Sr/^{86}Sr$ ratios are remarkably lower than those of all other metasedimentary rock in the region, from schist to migmatite (Fig. 10, see also Rapela et al., 1998). In particular for aluminous granulites, this observation is problematic as experimental constraints, mineral evolution and geochemical data consistently point to the idea that Grt–Crd granulites derived from a sedimentary protolith whose composition is retained by unmelted gneisses. This observed isotopic difference could reflect other processes, such as isotopic disequilibrium during melting and formation of the restitic granulites (e.g. Barbero et al., 1995; Knesel and Davidson, 1996). These authors show that Sr-isotopic disequilibrium occurs if felsic partial melts leave the source at a rate rapid enough to impede homogenization of $^{87}Sr/^{86}Sr$ ratios between source minerals and melt through ion self-diffusion. In their experiment, Knesel

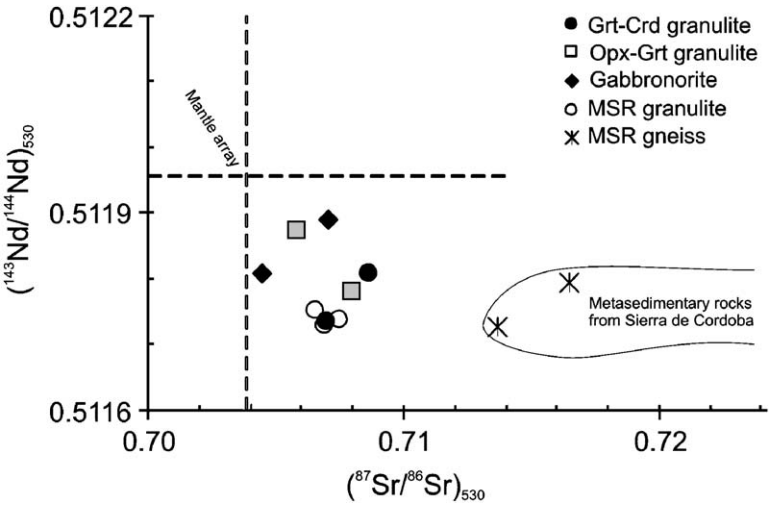

Fig. 10. Plot of Nd vs Sr isotopic ratios at 530 Ma for granulites and gabbronorites. Data for Santa Rosa Massif (MSR) samples and Cambrian metasedimentary rocks (from Rapela et al., 1998) are shown for comparison.

and Davidson (1996) proved that the breakdown of biotite with very high Rb/Sr and $^{87}Sr/^{86}Sr$ ratios produces melts enriched in $^{87}Sr/^{86}Sr$ ratio with respect to their source. Thus, when a partial melt with high Rb/Sr and $^{87}Sr/^{86}Sr$ ratios is drained from the source in a time scale shorter than the time necessary to reach isotopic ($^{87}Sr/^{86}Sr$ ratio) equilibration with residual phases (see calculation in Knesel and Davidson, 1996), the residuum acquires a $^{87}Sr/^{86}Sr$ ratio lower than its protolith. Although this particular result is obtained only when the stoichiometry of melting leads to the consumption of biotite at a much higher rate than plagioclase (e.g. Barbero et al., 1995), the mechanism for production of isotopic disequilibrium is well demonstrated and may explain the lower initial $^{87}Sr/^{86}Sr$ ratios (<0.708) in the restitic granulites compared to those from their putative sources (>0.713; see Fig. 10). This argument is also consistent with the conclusion that during the melting event that generated the granulites, biotite was consumed whereas plagioclase persisted by becoming more calcic. Furthermore, independent evidence that the granulites formed by a short-lived event caused by a local thermal input (Otamendi et al., 2005) enhances the possibility that melting was rapid enough to trigger isotopic disequilibrium.

Considered together the lithologies display an erratic and somewhat mixed sequence of Sr- and Nd-isotopic composition that renders hard to distinguish among gabbronorites, intermediate granulites and aluminous granulites by their isotopic signature (Figs. 6C and 10). The isotopic composition of gabbronorites with low εNd and high $^{87}Sr/^{86}Sr$ ratios positively reflects the incorporation of radiogenic material into the mafic rocks. This observation ultimately indicates that the gabbronorites are hybrid in origin. General and particular aspects of this sort of contamination of mafic magmas have been explained for the vast mafic body from Ivrea Zone (Voshage et al., 1990). Notably, within the mafic complex from Ivrea, mantle-like isotopic compositions occur only in ultramafic cumulate that formed in the lower levels of a large magmatic chamber (Voshage et al., 1990). Hence, we would not expect to find mantle-like isotopic ratios in the study case as mafic rocks are largely subordinate to supracrustal rocks. One of the two analysed Opx–Grt granulites presents an isotopic composition that is indistinguishable from those of the gabbronorites (Fig. 10), so reflecting that either the mafic magmas were largely hybridized with a material similar to the Opx–Grt granulites or some Opx–Grt granulites are partly made up by igneous mafic materials. Although none of the two possibilities may be categorically ruled out, the second one finds some support in the relative abundance of trace elements previously discussed.

5.5. Implications for the geochemical character of crustal melting residues

Several petrologic and geochemical lines of evidence suggest that the studied Grt–Crd granulites may have been generated as residues of crustal melting. However, it has not been ruled out the alternative that, as many other Crd–Ath–Opx-bearing granulites, the studied aluminous granulites inherited the chemistry of extensively weathered sedimentary protoliths (e.g. Moore and Waters, 1990). REE abundance provides hints to elucidate this issue. Studied aluminous granulites differ from common Crd–Ath–Opx-bearing granulites in that they are significantly depleted in LREE, and somewhat enriched in HREE. Excluding Eu^{+2}, REE have very similar ionic potential, so that REE could not be separated by any process that just involves water–solid interaction. For this reason, most sedimentary rocks show REE patterns largely resembling the upper crustal abundances of REE (e.g. McLennan, 1989). Hence, weathering does not appear to fractionate REE to make the REE pattern of aluminous granulites from any either igneous or sedimentary typical rocks. Moreover, the low abundance of Th, an element that has high ionic potential, is also inconsistent with Grt–Crd granulites consisting of sedimentary residue from intensive weathering. Elemental fractionation by interaction between fluid and solid cannot easily account for the V-shaped REE pattern of aluminous granulites (Fig. 4A). By contrast, it is below explained why the REE abundance in these granulites could be regarded as resulting from partial melting and granulitic residue formation.

A lower than expected depletion of incompatible elements in granulites has been recognized as evidence of incomplete segregation of melts from the residues (e.g. Rudnick and Presper, 1990), however the incompatible element contents of the residual granulites studied here suggest efficient melt extraction. The low abundance of LREE in the granulites, which depend on the degree to which monazite is dissolved into a coexisting anatectic melt (e.g. Montel, 1996), reflects the absence of a significant amount of unsegregated melt. Moreover, the granulites are depleted in elements having a lithophile character such as Li, Cs, Ba, and Th. Specifically, the behaviour of Th contrast with the high concentrations of Zr (300–500 ppm) implying that zircon and other rock-forming minerals were unable to sequester significant amounts of Th released after

monazite breakdown (see Villaseca et al., 2003). Complementary to this, those elements that are compatible in residual phases are enriched in the granulites. Almost surely Sc is significantly enriched (15–34 ppm) in the aluminous granulites due to the important proportion of Sc contained in garnets (Otamendi et al., 2002). This feature could also explain the enrichment in HREE and Y in the garnet-bearing granulites.

Granulite-facies rocks normally have low bulk K abundances and high K/Rb ratios (e.g. Rudnick and Presper, 1990). In terranes preserving the transition from amphibolite- to granulite-facies, these geochemical traits become stronger with increasing metamorphic grade (Schnetger, 1994; Hansen et al., 2002). These studies also reached the conclusion that more than one petrologic process may give rise to this geochemical trend. In fact, comparison of aluminous granulites with amphibolite- to granulite-facies gneisses and migmatites from the supracrustal sequence from the Sierra de Comechingones (Otamendi and Patiño Douce, 2001) shows that the range of Rb abundances and K/Rb ratios does not change significantly with decreasing K content (Fig. 11A). Given that there are several lines of evidence supporting a residual origin for the aluminous granulites, the lack of high K/Rb ratios is puzzling. We consider here that the extreme depletion in K accompanied by low K/Rb ratios is due to the breakdown of primary biotite without producing K-feldspar. The principles underlying this argument are presented in Fig. 11B and treated in the following discussion. For the study case (e.g. Otamendi and Patiño Douce, 2001) the rate of biotite consumption with melting progress can be reasonably fitted with a linear equation ($Bt = -0.5F + 0.3$, where Bt and F denote weight fraction of biotite and melt, respectively). This result enables us to appraise the total amount of biotite being consumed at a given partial melting fraction. According to the model melting reaction (R1) the amount of K and Rb in the melt is mostly supplied by biotite destruction. If all melt is removed from the source, the residuum suffers a strong depletion in K abundance and a small decrease of the K/Rb ratio (path I in Fig. 11B), potentially explaining the first order K and K/Rb ratio characteristics of the granulite. In contrast, if some melt fraction is unable to leave the source and remains interstitially among peritectic phases, K-feldspar crystallizes within the residual assemblage. We model an evolution path (path II in Fig. 11B) assuming that half of the melt leaves the source and that all the K contained in the retained melt is used to form K-feldspar. This model produces a strong increase of K/Rb ratio and a slight decrease of absolute K in the residue. This evolution is

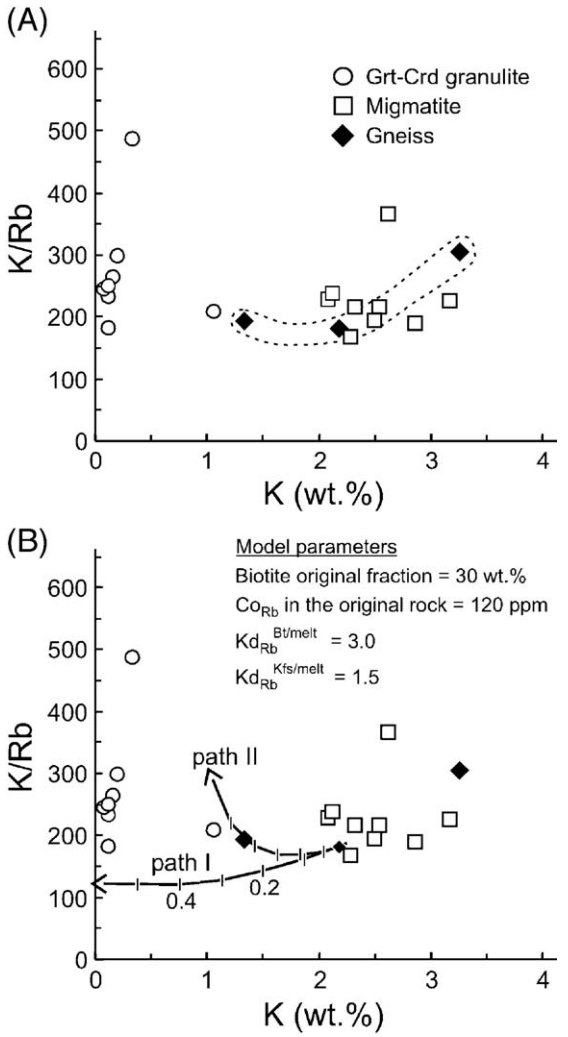

Fig. 11. (A) K/Rb vs K variations for the northern Sierra de Comechingones metamorphic rocks. Bulk rock compositions of migmatites and gneisses are taken from Otamendi and Patiño Douce (2001) and unpublished data. (B) Quantitative illustration of the effects of different evolution processes on the K/Rb ratio and total K content in the residues left after partial melting. Modelling considers two cases that differ only in how much melt is extracted from the source. Path I: all melt escapes, leaving a melt-free residuum. Path II: one half of the produced melt escapes, whereas the other half remains mixed in the residue and crystallizes in situ. Compositional trends in the residues are shown by tick marks giving the fraction of melt (from 0.1 to 0.5) produced during partial melting. Partition coefficients (Kd) are representative values taken from Rollinson (1993). See text for further details and assumptions.

a consequence of the fact that for Rb the mineral/melt partition coefficient of K-feldspar is normally lower than that of biotite, while the content of K (e.g. K_2O wt.%) is higher in the K-feldspar than in biotite. Thus, the lack of enrichment of K/Rb ratios in low K granulites, such as those studied here, ultimately reflects that melts were extensively segregated from residues,

without leaving significant K-feldspar in the residue. The small range in K/Rb ratios observed among the Grt–Crd granulites (Fig. 11) may be attributable to either variability in protoliths chemistry, or to the effect produced by residual plagioclase, as this phase accepts relatively little K and Rb into its structure but retains more K than Rb and therefore has a K/Rb ratio much higher than coexisting biotite (Rudnick, 1992).

6. Conclusions

The primary conclusion of this work is that the studied aluminous Grt–Crd granulites are the residuum left after by partial melting of rocks similar to the surrounding metasedimentary gneisses. A wide variety of field, petrographic, phase–equilibria relationships, and major and trace elements support this origin. More generally, these results support the concept of a granulite–granite connection, whereby lithophile-enriched peraluminous felsic granitoids in the upper crust are complementary to refractory granulitic residues at depth. The process of melting crustal rocks and allowing the felsic melts to separate and migrate upward has been considered to be a major process in differentiating the crust (Vielzeuf et al., 1990; Clemens, 1990). However, the majority of the granulites exposed at the Earth's surface do not appear to have trace element characteristics that unquestionably reflect an origin as residues left after removal of granite melt. This problem was addressed by Rudnick and Presper (1990), who estimated that moderate amounts of non-drained melts could erase the residual trace element signature of restitic granulites. If this explanation is correct, then the degree to which granulites residing at deep crustal levels are depleted in a felsic melt component becomes unclear, and the effectiveness of the granulite–granite connection as an intracrustal differentiation process is called into question. This problem deserves further study.

Additionally, a suite of mafic rocks have intruded and interacted with the aluminous granulites, giving rise to a distinctive group of intermediate Opx–Grt granulites by mixing and melting. The results of our studies show that processes other than simple melting and melt extraction can play a role in the formation of granulites, and that the interaction of these processes leaves complex petrologic features and geochemical patterns in the rocks. Granulites therefore require thorough study in order to sort out how different petrologic processes have interacted to produce the range of petrological, geochemical, and isotopic features. This study suggests that some granulites are open systems not only in the sense of losing felsic melt upward, however in incorporating mafic melts from below. In particular, our results support the view that the presence of Opx- and Grt-bearing granulites should be considered with awareness that at least some of them could have been formed by the interaction of mantle-derived mafic magmas with metasedimentary rocks (e.g. Patiño Douce, 1995).

Acknowledgements

This work was funded by ANPCYT-Argentina grant PICT 7-7193, CONICET grant PEI 6548, and by a complementary grant from SeCyT-UNRC. J.O and A.T. are supported by CONICET (Argentina). The manuscript benefited from critical reviews by two anonymous reviewers who gave us the opportunity to clarify and strengthen the ideas presented here. We acknowledge C. Villaseca and A. Garcia Casco for a very helpful review of a draft version of the work. The manuscript was substantially improved both in language style and science by L.P. Gromet to whom we are deeply indebted for this complicated and very productive undertaking.

Appendix A. Supplementary data

Supplementary data associated with this article can be found, in the online version, at doi:10.1016/j.lithos.2005.09.007.

References

Barbero, L., Villaseca, C., Rogers, G., Brown, P.E., 1995. Geochemical and isotopic disequilibrium in crustal melting: an insight from the anatectic granitoids from Toledo, Spain. J. Geophys. Res. 100, 15745–15765.

Berman, R.G., 1988. Internally-consistent thermodynamic data for minerals in the system Na_2O–K_2O–CaO–MgO–FeO–Fe_2O_3–Al_2O_3–SiO_2–TiO_2–H_2O–CO_2. J. Petrol. 29, 445–522.

Berman, R.G., Aranovich, L.Ya., 1996. Optimized standard state and solution properties of minerals: I. Model calibration for olivine, orthopyroxene, cordierite, garnet, and ilmenite in the system FeO–MgO–CaO–Al_2O_3–TiO_2–SiO_2. Contrib. Mineral. Petrol. 126, 1–24.

Burnham, C.W., 1979. The importance of volatile constituents. In: Yoder, H.S. (Ed.), The Evolution of the Igneous Rocks: Fiftieth Anniversary Perspectives. Princeton University Press, Princeton, pp. 439–482.

Brown, G.C., Fyfe, W.S., 1970. The production of granitic melts during ultrametamorphism. Contrib. Mineral. Petrol. 28, 310–318.

Brown, M., 1994. The generation, segregation, ascent and emplacement of granite magma: the migmatite-to-crustally-derived granite connection in thickened orogens. Earth-Sci. Rev. 36, 83–130.

Clemens, J.D., 1990. The granulite–granite connection. In: Vielzeuf, D., Vidal, Ph. (Eds.), Granulites and Crustal Evolution. Kluwer Academic Publishers, Dordrecht, pp. 25–36.

Clemens, J.D., Wall, V.J., 1981. Origin and crystallization of some peraluminous (S-type) granitic magmas. Can. Mineral. 19, 111–131.

Conrad, W.K., Nicholls, I.A., Wall, V.J., 1988. Water-saturated and -undersaturated melting of metaluminous and peraluminous crustal compositions at 10 kb: evidence for the origin of silicic magmas in the Taupo Volcanic Zone, New Zealand, and other occurrences. J. Petrol. 29, 765–803.

de la Rosa, J.D., Chacón, H., Sánchez de la Campa, A., Carrasco, R., Nieto, J.M., 2001. Metodología y análisis de elementos trazas-REE mediante ICP-MS del standard SARM 1 (granito) y SARM 4 (norita). In: Lago, M., Arranz, E., Galé, C. (Eds.), Libro de Actas del III Congreso Ibérico de Geoquímica. Zaragoza, España, pp. 435–438.

Dostal, J., Keppie, D.J., Jutras, P., Millar, B.V., Murphy, B.J., 2006. Evidence for the granulite–granite connection: penecontemporaneous high-grade metamorphism, granitic magmatism and core complex development in the Liscomb Complex, Nova Scotia, Canada. Lithos 86, 77–90.

Faure, G., 1986. Principles of Isotope Geology, 2nd ed. John Wiley & Sons, pp. 1–589.

Frost, B.R., Frost, C.D., 1987. CO_2, melts and granulite metamorphism. Nature 327, 503–506.

Gordillo, C.E., 1984. Migmatitas cordieríticas de la Sierra de Córdoba, condiciones físicas de la migmatización. Misc. - Acad. Nac. Cienc. 68, 1–40.

Hansen, E., Ahmed, K., Harlov, D., 2002. Rb depletion in biotites and whole rocks across an amphibolite to transition zone, Tamil Nadu, South India. Lithos 64, 27–47.

Harlov, D., Förster, H.-J., 2002. High-grade fluid metasomatism on both a local and a regional scale: the Seward Peninsula, Alaska, and the Val Strona di Omegna, Ivrea–Verbano Zone, northern Italy: Part I. petrography and silicate mineral chemistry. J. Petrol. 43, 769–799.

Knesel, K.M., Davidson, J.P., 1996. Isotopic disequilibrium during melting of granite and implications for crustal contamination of magmas. Geology 24, 243–246.

Kretz, R., 1983. Symbols for rock-forming minerals. Am. Mineral. 68, 277–279.

Martino, R., Escayola, M., Saal, A., 1994. Estructura del cuerpo de "kinzigita" del Río Santa Rosa, Departamento Calamuchita, Provincia de Córdoba. Rev. Asoc. Geol. Argent. 49, 3–10.

McLennan, S.M., 1989. Rare earth elements in sedimentary rocks: influence of provenance and sedimentary processes. In: Lipin, B.R., McKay, G.A. (Eds.), Rare Earth Elements, Reviews in Mineralogy, vol. 21, pp. 169–200.

Montel, J.M., 1996. A model for monazite/melt equilibrium and application to the generation of granitic magmas. Chem. Geol. 110, 127–146.

Montero, P., Bea, F., 1998. Accurate determination of Rb^{87}/Sr^{86} and Sm^{147}/Nd^{144} ratios by inductively coupled plasma mass spectrometry in isotope geoscience: an alternative to isotope dilution analysis. Analyt. Chim. Acta 358, 227–233.

Moore, J.M., Waters, D., 1990. Geochemistry and origin of cordierite-orthoamphibole/orthopyroxene-phlogopite rocks from Namaqualand, South Africa. Chem. Geol. 85, 77–100.

Lambert, I.B., Heier, K.S., 1967. Geochemical investigation of deep-seated rocks in the Australian shield. Lithos 1, 30–53.

Le Breton, N., Thompson, A.B., 1988. Fluid-absent (dehydration) melting of biotite in metapelites in the early stages of crustal anatexis. Contrib. Mineral. Petrol. 99, 226–237.

Otamendi, J.E., Patiño Douce, A.E., 2001. Partial melting of aluminous metagreywackes in the northern Sierra de Comechingones, Central Argentina. J. Petrol. 42, 1751–1772.

Otamendi, J.E., Patiño Douce, A.E., Demichelis, A.H., 1999. Amphibolite to granulite transition in aluminous greywackes from the Sierra de Comechingones, Córdoba, Argentina. J. Metamorph. Geol. 17, 415–434.

Otamendi, J.E., de la Rosa, J.D., Patiño Douce, A.E., Castro, A., 2002. Rayleigh fractionation of heavy rare earth and yttrium during metamorphic garnet growth. Geology 30, 159–162.

Otamendi, J.E., Tibaldi, A.M., Demichelis, A.H., Rabbia, O.M., 2005. Metamorphic evolution of the Río Santa Rosa Granulites, northern Sierra de Comechingones, Argentina. J. South Am. Earth Sci. 18, 163–181.

Patiño Douce, A.E., 1995. Experimental generation of hybrid silicic melts by reaction of high-Al basalt with metamorphic rocks. J. Geophys. Res. 100, 15623–15639.

Patiño Douce, A.E., 1996. Effects of pressure and H_2O content on the compositions of primary crustal melts. Trans. R. Soc. Edinb. Earth Sci. 87, 11–21.

Patiño Douce, A.E., Beard, J.S., 1995. Dehydration-melting of biotite gneiss and quartz amphibolite from 3 to 15 kbar. J. Petrol. 36, 707–738.

Patiño Douce, A.E., Johnston, A.D., 1991. Phase equilibria and melt productivity in the pelitic system: implications for the origin of peraluminous granitoids and aluminous granulites. Contrib. Mineral. Petrol. 107, 202–218.

Powell, R., 1983. Fluids and melting under amphibolite facies conditions. J. Geol. Soc. Lond. 140, 629–633.

Rapela, C.W., Pankhurst, R.J., Casquet, C., Baldo, E., Saavedra, J., Galindo, C., Fanning, C.M., 1998. The Pampean Orogeny of the southern proto-Andes: Cambrian continental collision in the Sierras de Córdoba. In: Pankhurst, R.J., Rapela, C.W. (Eds.), The Proto-Andean Margin of Gondwana, Special Publications, vol. 142. Geological Society, London, pp. 181–217.

Rollinson, H.R., 1993. Using Geochemical Data: Evaluation, Presentation, Interpretation. Longman Scientific & Technical, UK, pp. 1–352.

Rollinson, H.R., Tarney, J., 2005. Adakites — the key to understanding LILE depletion in granulites. Lithos 79, 61–81.

Rudnick, R.L., 1992. Restites, Eu anomalies, and the lower continental crust. Geochim. Cosmochim. Acta 56, 963–970.

Rudnick, R.L., Presper, T., 1990. Geochemistry of intermediate to high pressure granulites. In: Vielzeuf, D., Vidal, Ph. (Eds.), Granulites and Crustal Evolution. Kluwer Academic Publishers, Dordrecht, pp. 523–550.

Sawyer, E.W., 1998. Formation and evolution of granite magmas during crustal reworking: the significance of diatexis. J. Petrol. 39, 1147–1167.

Schnetger, B., 1994. Partial melting during the evolution of the amphibolite- to granulite-facies gneisses of the Ivrea Zone, northern Italy. Chem. Geol. 113, 71–101.

Spear, F.S., 1993. Metamorphic phase equilibria and pressure–temperature-time paths. Mineral. Soc. Am., Monograph Series, Washington, pp. 1–799.

Stevens, G., Clemens, J.D., Droop, G.T.R., 1997. Melt production during granulite-facies anatexis: experimental data from "primitive" metasedimentary protoliths. Contrib. Mineral. Petrol. 128, 352–370.

Taylor, S.R., McLennan, S.M., 1985. The Continental Crust: Its Composition and Evolution. Blackwell Scientific Publications, Oxford, pp. 1–312.

Thompson, A.B., 1982. Dehydration melting of pelitic rocks and the generation of H_2O-undersaturated granitic liquids. Am. J. Sci. 282, 1567–1595.

Vielzeuf, D., Holloway, J.R., 1989. Experimental determination of fluid-absent melting relations in the pelitic system. Consequences for crustal differentiation. Contrib. Mineral. Petrol. 98, 257–276.

Vielzeuf, D., Montel, J.M., 1994. Partial melting of metagreywackes: Part I. Fluid-absent experiments and phase relationships. Contrib. Mineral. Petrol. 117, 375–393.

Vielzeuf, D., Clemens, J.D., Pin, C., Moinet, E., 1990. Granites, granulites and crustal differentiation. In: Vielzeuf, D., Vidal, Ph. (Eds.), Granulites and Crustal Evolution. Kluwer Academic Publishers, Dordrecht, pp. 59–85.

Villaseca, C., Martín Romera, C., de la Rosa, J., Barbero, L., 2003. Residence and redistribution of REE, Y, Zr, Th and U during granulite-facies metamorphism: behaviour of accessory and major phases in peraluminous granulites of central Spain. Chem. Geol. 200, 293–323.

Voshage, H., Hofmann, A.W., Mazzucchelli, M., Rivalenti, G., Sinigoi, S., Raczek, I., Demarchi, G., 1990. Isotopic evidence from the Ivrea Zone for a hybrid lower crust formed by magmatic underplating. Nature 347, 731–736.